

# UAV Trajectory and Communication Co-design: Flexible Path Discretization and Path Compression

Yijun Guo, *Member, IEEE*, Changsheng You, *Member, IEEE*,  
Changchuan Yin, *Senior Member, IEEE*, and Rui Zhang, *Fellow, IEEE*

## Abstract

The performance optimization of UAV communication systems requires the joint design of UAV trajectory and communication efficiently. To tackle the challenge of infinite design variables arising from the continuous-time UAV trajectory optimization, a commonly adopted approach in the existing literature is by approximating the UAV trajectory with piecewise-linear path segments connected via a finite number of waypoints in three-dimensional (3D) space. However, this approach may still incur prohibitive computational complexity in practice when the UAV flight period/distance becomes long, as the distance between consecutive waypoints needs to be kept sufficiently small to retain high approximation accuracy. To resolve this fundamental issue, we propose in this paper a *new* and *general* framework for UAV trajectory and communication co-design with flexible number of waypoint optimization variables (called *designable* waypoints) or their *sub-path* representations. First, we propose a *flexible path discretization* scheme that optimizes only a number of selected waypoints (designable waypoints) along the UAV path for complexity reduction, while all the designable and non-designable waypoints are used in calculating the approximated communication utility along the UAV trajectory for ensuring high trajectory discretization accuracy. Next, given any number of designable waypoints, we propose a novel *path compression* scheme where the UAV 3D path is first decomposed into three one-dimensional (1D) sub-paths and each sub-path is then approximated by superimposing a number of selected basis paths (which are generally less than the number of designable waypoints) weighted by their corresponding path coefficients, thus further reducing the path design complexity. Finally, we provide a case study on UAV trajectory design for aerial data harvesting from distributed ground sensors, and numerically show that the proposed flexible path discretization and path compression schemes can significantly reduce the UAV trajectory design complexity yet achieve favorable rate performance as compared to conventional path/time discretization schemes.

## Index Terms

Unmanned aerial vehicle (UAV), trajectory and communication co-design, trajectory discretization, path compression.

Y. Guo and C. Yin are with the Beijing Key Laboratory of Network System Architecture and Convergence, Beijing University of Posts and Telecommunications, (email: {guoyijun, ccyin}@bupt.edu.cn).

C. You and R. Zhang are with the Department of Electrical and Computer Engineering, National University of Singapore (email: {eleyou, elezhang}@nus.edu.sg).

## I. INTRODUCTION

Unmanned aerial vehicle (UAV) has emerged as a new promising communication platform in future wireless systems/networks, thanks to its great advantages such as controllable maneuver, high mobility, on-demand and flexible deployment, as well as line-of-sight (LoS) dominant UAV-ground channels [1]. These appealing advantages have spurred fast-growing enthusiasm in both academia and industry recently, giving rise to a proliferation of new applications, such as UAV-enabled relaying [2]–[5], UAV-enabled data harvesting and dissemination [6]–[11], UAV-enabled wireless power transfer [12], [13], cellular-connected UAV [14]–[16], among others.

Particularly, for high-mobility UAV, its trajectory design has been extensively studied in the literature for maximizing various communication utilities (e.g., throughput, coverage, energy efficiency, and so on) under different UAV-ground channel models. For example, for UAV at high altitude in rural areas, the LoS UAV-ground channel model is practically accurate and thus has been widely used to design the two-dimensional (2D) UAV trajectory with fixed (minimum) UAV altitude (see, e.g., [6]–[9], [17], [18]). While for UAV in urban areas with dense buildings, the simplified LoS UAV-ground channel model fails to capture the non-negligible multi-path fading and shadowing effects, thus two more sophisticated channel models have been proposed in the literature to improve the accuracy, namely, the elevation-angle dependent Rician fading channel model [10] which is suitable for UAV operating at high altitude, and the (generalized) probabilistic LoS channel model [11] which is applicable to UAV at lower altitude. Under these two refined channel models, the three-dimensional (3D) UAV trajectory design has been studied for enhancing UAV communication performance by judiciously controlling the UAV-ground distance and elevation angle (both dependent on the UAV-ground horizontal and vertical distances) [10], [11]. Note that compared to quasi-static UAV placement design (see, e.g., [4], [19]–[22]) for which only a finite number of static UAV locations need to be optimized, UAV trajectory design generally is much more challenging since it involves *continuous time* that results in an *infinite* number of design variables associated with UAV trajectory as well as communication. A practical approach to tackle this problem is by approximating the UAV trajectory with a tractable *piecewise-linear continuous* trajectory where the path comprises consecutive line segments connected via a *finite* number of waypoints in 3D, while the time duration that the UAV spends on each line segment can be different. This scheme is referred to as the *conventional path discretization* (CPD) in this paper. Besides, another widely-used trajectory discretization scheme, called *time discretization* (TD), can be regarded as a special case of CPD with *identical* time-slot length over all line segments. To ensure sufficiently high trajectory discretization accuracy for the UAV-ground communication performance, it is required that for both CPD and TD

schemes, their adopted segment lengths should be no larger than a certain threshold such that the UAV-ground distance can be regarded as approximately unchanged within each line segment.

The above two trajectory discretization schemes, however, may entail a large number of line segments in practice when the UAV flight distance/period becomes long, thus resulting in prohibitive computational complexity for the 2D/3D UAV trajectory design. Moreover, to address the coupling between UAV trajectory and communication designs, a commonly adopted approach in the existing literature is by using the block coordinate descent (BCD) method to decouple the joint optimization via alternately optimizing UAV trajectory and communication in an iterative manner, which incurs additional computational complexity. These issues have motivated active research efforts recently to reduce the UAV trajectory design complexity [11], [13], [23]–[27]. For example, a low-complexity receding-horizon based optimization method was proposed in [23] that progressively designs the overall UAV trajectory with a moving time-window. Specifically, different from TD that imposes equal time-slot length on all line segments, the authors proposed to divide the entire time horizon into three sub-horizons with different time-slot lengths so as to reduce the number of design variables in each time-window. Alternatively, to maximize the UAV flight time given fixed propulsion energy supply, a customized low-complexity UAV trajectory design was proposed in [24] that optimizes only a UAV trajectory fragment in a short time horizon, while it treats the overall trajectory as the rotated and replicated ones of the trajectory fragment with certain rotation angles. In [25], the authors proposed to fit the UAV trajectory over time by finite Fourier series with TD, based on which the complicated UAV waypoint optimization can be reduced into finding optimal values of finite Fourier series coefficients. In [13], the authors considered the one-dimensional (1D) UAV trajectory and transformed the waypoint optimization problem into optimizing UAV hovering locations and durations by leveraging its optimal hover-and-fly structure. Besides, a hybrid offline-online optimization framework was developed in [11] to reduce the real-time trajectory design complexity, which first solves a time-consuming path optimization problem in the offline phase and then refines the UAV flying speeds and communication scheduling in the online phase by solving a low-complexity linear programming (LP). On the other hand, to reduce the complexity arising from the BCD method, an initial attempt has been made in [26] that simultaneously optimizes UAV trajectory and transmit power allocation. In addition, the alternating direction method of multipliers (ADMM) method was applied in [27] to decouple the joint optimization and obtain closed-form solutions to corresponding subproblems for reducing the computational complexity. Nevertheless, in view of the above works, there still lacks a *general* framework to reduce the complexity of UAV trajectory and communication co-design from the perspective of trajectory discretization/compression, which thus motivates our current work as the

first attempt to fill this gap, to the authors' best knowledge.

To this end, we first formulate a generic optimization problem to maximize the UAV communication utility by jointly designing the continuous-time UAV trajectory and communication. We then consider the piecewise-linear UAV trajectory for tractability and revisit the existing CPD and TD schemes as well as discuss their practical implementation issues. Next, to reduce the computational complexity of the CPD and TD schemes with practically large number of line segments, we propose a new and general framework that is able to reduce the number of (trajectory and communication) design variables in both the *time* and *spatial* domains. The main contributions of this paper are summarized as follows.

- Firstly, we propose a novel *flexible path discretization* (FPD) scheme to reduce the number of waypoints that need to be optimized over time in the CPD scheme. Specifically, we divide the waypoints required for ensuring desired trajectory discretization accuracy into two exclusive sets, namely, *designable* and *non-designable* waypoints. Among them, only the designable waypoints are optimized for reducing the UAV trajectory design complexity, while all the waypoints (including both designable and non-designable ones) are used in calculating the approximated utility and constraint functions to retain high trajectory discretization accuracy. Moreover, we show that the proposed FPD scheme in general entails fewer (designable) waypoints for trajectory representation as compared to TD and CPD schemes.
- Secondly, given any number of (designable) waypoints, we propose another alternative method, called *path compression* (PC), to further reduce the number of UAV trajectory design variables in the spatial domain. To this end, we first show that the UAV 3D path can be equivalently decomposed into three 1D sub-paths in the three coordinates, respectively, each of which can be represented by a superposition of the same number of basis paths as that of the time-domain waypoints, weighted by their corresponding path coefficients. Based on this result, we then propose a simple yet efficient PC method to approximate each sub-path with a reduced number of properly selected basis paths and their corresponding designable path coefficients, thus further reducing the design complexity of the FPD/CPD/TD schemes.
- Finally, we provide a case study to show different formulations of the same trajectory and communication co-design problem for the application of UAV-enabled data harvesting from distributed sensors under different trajectory discretization schemes with/without PC. By analyzing their computational complexities for solving their respective optimization problems, we show that compared to TD and CPD schemes, the UAV trajectory and communication co-design with the proposed FPD scheme achieves much lower complexity, which can be further reduced when combined with

Table I: List of main symbols/abbreviations and their meanings.

$I$	Number of constraints
$N$	Number of segments by conventional path discretization
$M$	Number of segments by time discretization
$L$	Number of long-segments by flexible path discretization
$J$	Number of short-segments within each long-segment by flexible path discretization
$N_{\text{FPD}}$	Number of all short-segments by flexible path discretization
$K$	Number of selected basis paths for path compression
$U, \bar{U}$	Communication utility function and its finite-sum approximation
$f, \bar{f}$	Constraint function and its finite-sum approximation
TD	Time discretization
CPD	Conventional path discretization
FPD	Flexible path discretization
PC	Path compression
FPD-PC	Flexible path discretization with path compression

the proposed PC scheme. Moreover, the proposed FPD and PC schemes also achieve favorable max-min rate performance as compared to TD and CPD schemes.

The remainder of this paper is organized as follows. Section II introduces the generic problem formulation and existing trajectory discretization schemes. Then, the proposed FPD and PC schemes are presented in Sections III and IV, respectively. A case study of UAV trajectory design for aerial data harvesting from distributed sensors is provided in Section V, followed by the corresponding simulation results given in Section VI. Finally, the conclusions are drawn in Section VII. For ease of reference, we summarize in Table I the main symbols and abbreviations used in this paper.

## II. PROBLEM FORMULATION AND TRAJECTORY DISCRETIZATION

### A. Generic Problem Formulation

The performance optimization of UAV communication systems in general requires the joint design of UAV trajectory and communication. Without loss of generality, let  $\mathcal{Q}(t)$  denote the UAV trajectories of all UAVs over time  $t \in [0, T]$  with  $T$  denoting the total UAV flight period, and  $\mathcal{R}(t)$  represent all relevant variables associated with the communication design over time  $t$ , such as communication scheduling, bandwidth and transmit power allocation, beamforming, etc. Then, a generic optimization problem for maximizing the UAV communication utility via jointly designing UAV trajectory and communication can be formulated as follows [1].

$$(P1) : \max_{\mathcal{Q}(t), \mathcal{R}(t)} U(\mathcal{Q}(t), \mathcal{R}(t))$$

$$\text{s.t.} \quad f_i(\mathcal{Q}(t)) \leq 0, \quad i = 1, \dots, I_1, \quad (1a)$$

$$h_i(\mathcal{R}(t)) \leq 0, \quad i = 1, \dots, I_2, \quad (1b)$$

$$g_i(\mathcal{Q}(t), \mathcal{R}(t)) \leq 0, \quad i = 1, \dots, I_3, \quad (1c)$$

where  $U(\mathcal{Q}(t), \mathcal{R}(t))$  denotes the communication utility function (such as communication throughput, energy efficiency, etc.) with respect to (w.r.t.) both UAV trajectory and communication variables in general;  $f_i(\mathcal{Q}(t)), i = 1, \dots, I_1$  represent the set of constraints on UAV trajectory only (e.g., maximum UAV speed);  $h_i(\mathcal{R}(t)), i = 1, \dots, I_2$  specify the set of constraints on UAV communication only; and  $g_i(\mathcal{Q}(t), \mathcal{R}(t)), i = 1, \dots, I_3$  denote the set of coupled constraints related to both UAV trajectory and communication. Problem (P1), in general, is difficult to be efficiently and optimally solved due to the following two main reasons. First, it involves continuous time  $t$  and thus results in an infinite number of UAV trajectory and communication design variables. Second, the UAV trajectory and communication design variables need to be jointly optimized, which usually renders problem (P1) a non-convex optimization problem and thus hard to be optimally solved.

To tackle the above difficulties, we can first apply the BCD method to decouple the joint optimization for UAV trajectory and communication. Specifically, by regarding  $\mathcal{Q}(t)$  and  $\mathcal{R}(t)$  as two blocks of design variables, the non-convex problem (P1) can be sub-optimally solved by using an iterative algorithm as follows. On one hand, given any feasible  $\mathcal{Q}(t) = \hat{\mathcal{Q}}(t)$ , problem (P1) is equivalent to

$$(P2) : \max_{\mathcal{R}(t)} U(\hat{\mathcal{Q}}(t), \mathcal{R}(t))$$

$$\text{s.t.} \quad h_i(\mathcal{R}(t)) \leq 0, \quad i = 1, \dots, I_2, \quad (2a)$$

$$g_i(\hat{\mathcal{Q}}(t), \mathcal{R}(t)) \leq 0, \quad i = 1, \dots, I_3, \quad (2b)$$

which reduces to the communication design problem only. By discretizing the time into a finite number of intervals (e.g., TD introduced later), problem (P2) can be efficiently solved by using existing techniques developed for wireless communication resource-allocation optimization over parallel channels (e.g., block-fading channels, orthogonal-frequency channels). On the other hand, given any feasible  $\mathcal{R}(t) = \hat{\mathcal{R}}(t)$ , problem (P1) reduces to

$$(P3) : \max_{\mathcal{Q}(t)} U(\mathcal{Q}(t), \hat{\mathcal{R}}(t))$$

$$\text{s.t.} \quad f_i(\mathcal{Q}(t)) \leq 0, \quad i = 1, \dots, I_1, \quad (3a)$$

$$g_i(\mathcal{Q}(t), \hat{\mathcal{R}}(t)) \leq 0, \quad i = 1, \dots, I_3, \quad (3b)$$

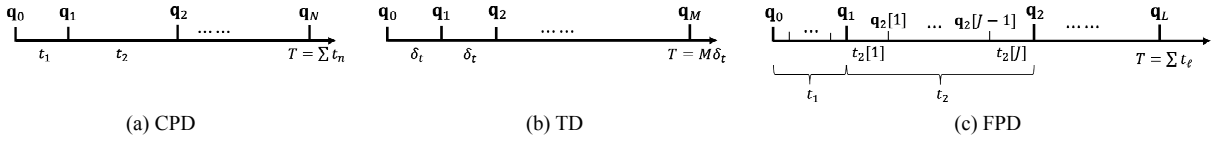


Fig. 1: Illustration of different piecewise-linear trajectory discretization schemes in 1D.

which needs to optimize the *continuous-time* UAV trajectory. For the purpose of exposition, we focus on the case with one single UAV only in this paper, where  $\mathcal{Q}(t) \triangleq \mathbf{q}(t)$  with  $\mathbf{q}(t)$  denoting the single-UAV 3D trajectory over time, while the proposed design framework and solutions can be extended to the general case with multiple UAVs (e.g., a swarm of UAVs). By slightly abusing the notations of  $U(\cdot)$  and  $f(\cdot)$ , problem (P3) can be equivalently rewritten as

$$\begin{aligned}
 \text{(P4)} : \quad & \max_{\mathbf{q}(t)} U(\mathbf{q}(t)) \\
 \text{s.t.} \quad & f_i(\mathbf{q}(t)) \leq 0, \quad i = 1, \dots, I,
 \end{aligned} \tag{4a}$$

where  $I = I_1 + I_3$ , and  $f_i(\mathbf{q}(t)), i = 1, \dots, I$  represent the set of constraints in (3a) and (3b) associated with UAV trajectory. Compared to problem (P2), problem (P4) is relatively new as well as more challenging to solve due to the continuous-time trajectory and trajectory-dependent communication utility/constraints. As such, we focus on solving problem (P4) in the rest of this paper.

### B. UAV Trajectory Discretization: Existing Schemes

1) *CPD*: The solution to problem (P4), in general, is intractable due to the infinite number of UAV trajectory variables over time, i.e.,  $\mathbf{q}(t)$ . To overcome this difficulty, we consider the tractable *piecewise-linear* continuous UAV trajectory as illustrated in Fig. 1(a), which can be characterized by a sequence of *ordered waypoints* along the UAV flying *path* with line segments connecting them, as well as the *traveling time duration* that the UAV spends on each line segment. Thereby, the UAV velocity (specifying both direction and speed) over each line segment is also determined if it is assumed to be constant over each line segment (but can change over different segments). Mathematically, let  $\{\mathbf{q}_n\}_{n=0}^N$  denote the  $N + 1$  (ordered) waypoints along the UAV path with  $\mathbf{q}_n \triangleq [q_{n,x}, q_{n,y}, q_{n,z}]^T$ . For each of the resultant  $N$  line segments, say, segment  $n$  that connects the waypoints  $\mathbf{q}_{n-1}$  and  $\mathbf{q}_n$ , we denote by  $t_n$  the UAV traveling duration over it. As such, the piecewise-linear continuous trajectory  $\mathbf{q}(t)$  can be fully characterized by  $\{\{\mathbf{q}_n\}_{n=0}^N, \{t_n\}_{n=1}^N\}$ , based on which, the constant UAV velocity over each segment  $n$ , denoted by  $\mathbf{v}_n$ , is given by  $\mathbf{v}_n \triangleq (\mathbf{q}_n - \mathbf{q}_{n-1})/t_n, n = 1, \dots, N$ . It is worth mentioning that the above piecewise-linear trajectory is also called *path discretization* in the existing literature [1], as the UAV

path is discretized into multiple line segments with flexible lengths and UAV traveling durations over them. We refer to this scheme as CPD in this paper for convenience.

Although much simplified, the functions of communication utility and constraints under the piecewise-linear continuous trajectory, i.e.,  $U(\mathbf{q}(t))$  and  $\{f_i(\mathbf{q}(t))\}$ , are still hard to obtain in closed-form for optimization in general, since they involve integrals w.r.t. the continuous UAV trajectory over each segment. An efficient approach to tackle this difficulty is via approximating the integral by a finite-sum. Taking the communication utility function as an example, its finite-sum approximation can be obtained as

$$U(\mathbf{q}(t)) = \int_0^T u(\mathbf{q}(t))dt \approx \sum_{n=1}^N t_n u(\mathbf{q}(\tau_n)) = \sum_{n=1}^N t_n u(\mathbf{q}_n) \triangleq \bar{U}_{\text{CPD}}(\{\mathbf{q}_n\}, \{t_n\}), \quad (5)$$

where  $u(\cdot)$  denotes the utility function associated with UAV locations,  $\mathbf{q}(\tau_n)$  denotes any UAV location over segment  $n$  (with  $\sum_{\tilde{n}=1}^{n-1} t_{\tilde{n}} \leq \tau_n \leq \sum_{\tilde{n}=1}^n t_{\tilde{n}}$ ) which is set as  $\mathbf{q}(\tau_n) = \mathbf{q}(\sum_{\tilde{n}=1}^n t_{\tilde{n}}) \triangleq \mathbf{q}_n$  without loss of generality, and  $\bar{U}_{\text{CPD}}(\cdot)$  represents the approximated communication utility function with CPD. To ensure sufficiently high finite-sum approximation accuracy, the length of each line segment, intuitively, should not exceed a certain threshold. To show this, we first present a useful lemma below that characterizes the finite-sum approximation error for the utility function given in (5).

**Lemma 1.** Let  $D_u = \max_{\mathbf{q} \in \mathbf{q}(t)} \|\nabla u(\mathbf{q})\|$  denote the maximum norm of the gradient of the utility function  $u(\mathbf{q}(t))$  given any feasible trajectory  $\mathbf{q}(t)$ , and assume that  $D_u$  exists and  $D_u < \infty$ . Then, given  $T$  and the maximum distance between consecutive waypoints for approximating the utility function given in (5), denoted by  $\Delta_{\text{max}}^U$ , the finite-sum approximation error is upper-bounded by

$$E_U = |U(\mathbf{q}(t)) - \bar{U}_{\text{CPD}}(\{\mathbf{q}_n\}, \{t_n\})| \leq \frac{1}{2} D_u \Delta_{\text{max}}^U T. \quad (6)$$

*Proof:* See Appendix A. □

With a prescribed maximum tolerable utility approximation error  $E_{U,\text{max}}$ ,  $\Delta_{\text{max}}^U$  should be set as

$$\Delta_{\text{max}}^U = \frac{2E_{U,\text{max}}}{TD_u}. \quad (7)$$

**Example 1.** Consider a UAV-enabled data harvesting system, where a UAV is dispatched to collect data from one ground sensor node (SN) located at  $\mathbf{w} \in \mathbb{R}^{3 \times 1}$ . Assuming the simplified LoS UAV-ground channel model, the communication utility, defined as the average achievable rate in bits per second per Hertz (bps/Hz) at the UAV within a flight period of  $T$ , is given by [7]

$$U(\mathbf{q}(t)) = \frac{1}{T} \int_0^T \log_2 \left( 1 + \frac{P\beta_0}{\|\mathbf{q}(t) - \mathbf{w}\|^2 \sigma^2} \right) dt, \quad (8)$$



where  $P$  denotes the SN's transmit power,  $\beta_0$  denotes the channel power gain at the reference distance of 1 meter (m), and  $\sigma^2$  is the receiver noise power at the UAV. With CPD and based on (5), the utility function in (8) can be approximated by

$$U(\mathbf{q}(t)) \approx \bar{U}_{\text{CPD}}(\{\mathbf{q}_n\}, \{t_n\}) = \frac{1}{T} \sum_{n=1}^N t_n \log_2 \left( 1 + \frac{P\beta_0}{\|\mathbf{q}_n - \mathbf{w}\|^2 \sigma^2} \right). \quad (9)$$

Then, as proved in Appendix B, for  $u(\mathbf{q}(t)) = \frac{1}{T} \log_2 \left( 1 + \frac{P\beta_0}{\|\mathbf{q}(t) - \mathbf{w}\|^2 \sigma^2} \right)$  and given the minimum UAV flight altitude  $H_{\min}$ , we have  $D_u = \frac{2c_2}{\ln 2} \frac{c_1}{(c_1^2 + H_{\min}^2)(c_1^2 + H_{\min}^2 + c_2)}$  where the constants  $c_1$  and  $c_2$  are defined in Appendix B. As such, given the maximum tolerable utility approximation error  $E_{U,\max}$ , the segment length should satisfy  $\|\mathbf{q}_n - \mathbf{q}_{n-1}\| \leq \Delta_{\max}^U = \frac{2E_{U,\max}}{TD_u}$ ,  $n = 1, \dots, N$ . Moreover, it can be shown that  $\Delta_{\max}^U$  monotonically increases with  $H_{\min}$ , which is expected since the UAV-ground distance changes more slowly when the UAV is at higher altitude.

By using the similar method as above, we can also obtain the maximum segment length associated with each constraint, which is denoted by  $\Delta_{\max}^{f_i}$ ,  $i = 1, \dots, I$ . With  $\Delta_{\max}^U$  and  $\{\Delta_{\max}^{f_i}\}$ , the maximum segment length that satisfies all the finite-sum approximation requirements can be obtained as  $\Delta_{\max} = \min\{\Delta_{\max}^U, \{\Delta_{\max}^{f_i}\}\}$ . As such, we have

$$\|\mathbf{q}_n - \mathbf{q}_{n-1}\| \leq \min\{\Delta_{\max}, t_n V_{\max}\}, \quad n = 1, \dots, N, \quad (10)$$

which incorporates the UAV maximum speed constraint under the CPD scheme with  $V_{\max}$  denoting the maximum UAV speed. Let  $\mathbf{q}_{\text{str}}$  and  $\mathbf{q}_{\text{end}}$  denote the start and end locations for the UAV trajectory (if specified). Then, if  $\mathbf{q}_{\text{str}} \neq \mathbf{q}_{\text{end}}$ , the number of line segments,  $N$ , should satisfy  $N \geq N_{\min} \triangleq \left\lceil \frac{\|\mathbf{q}_{\text{str}} - \mathbf{q}_{\text{end}}\|}{\Delta_{\max}} \right\rceil$ , where  $\lceil \cdot \rceil$  denotes the ceiling function and the equality holds when the UAV flies toward the end location following a straight-line path. Note that given  $T \geq \frac{\|\mathbf{q}_{\text{str}} - \mathbf{q}_{\text{end}}\|}{V_{\max}}$ , the UAV trajectory design becomes more flexible as  $T$  increases. Hence, we usually set  $N \gg N_{\min}$  when  $T$  is practically large.

Under the above finite-sum approximation for both the communication utility  $U(\mathbf{q}(t))$  and constraint functions  $\{f_i(\mathbf{q}(t))\}$ , problem (P4) can be approximately reformulated as

$$\begin{aligned} \text{(P5)} : \quad & \max_{\{\mathbf{q}_n\}, \{t_n\}} \quad \bar{U}_{\text{CPD}}(\{\mathbf{q}_n\}, \{t_n\}) \\ \text{s.t.} \quad & \bar{f}_{i,\text{CPD}}(\{\mathbf{q}_n\}, \{t_n\}) \leq 0, \quad i = 1, \dots, I, \end{aligned} \quad (11a)$$

where  $\{\bar{f}_{i,\text{CPD}}(\{\mathbf{q}_n\}, \{t_n\})\}$  denote the set of approximated constraints under the CPD scheme. Although problem (P5) is generally non-convex, the BCD and successive convex approximation (SCA) techniques

(as will be detailed in Section V) can be employed to solve it sub-optimally.

**Remark 1** (Practical implementation). Let  $\{\mathbf{q}_n^*\}$ , and  $\{t_n^*\}$  denote the optimized UAV waypoints and time durations by solving problem (P5), respectively, and  $\mathbf{q}^*(t)$  denote the piecewise-linear trajectory constructed from  $\{\{\mathbf{q}_n^*\}, \{t_n^*\}\}$ . It is worth noting that the attainable communication utility by following the designed trajectory  $\mathbf{q}^*(t)$  (i.e.,  $U(\mathbf{q}^*(t))$ ) may not be the same as the estimated one (i.e.,  $\bar{U}_{\text{CPD}}(\{\mathbf{q}_n^*\}, \{t_n^*\})$ ) due to the finite-sum approximation error, which, however, can be upper-bounded if the conditions in Lemma 1 are satisfied. Moreover, the constraints of  $f_i(\mathbf{q}^*(t)) \leq 0, i = 1, \dots, I$  may also be violated in practice. To address this issue, an efficient approach is to *proactively* introduce robustness to the constraints prior to optimization so as to reduce the constraint-violation probability in practical implementation. For instance, we can redefine the constraints as

$$(1 + \epsilon_i)\bar{f}_{i,\text{CPD}}(\{\mathbf{q}_n\}, \{t_n\}) \leq 0, \quad i = 1, \dots, I, \quad (12)$$

by setting the parameter  $\epsilon_i$  according to the prescribed finite-sum approximation accuracy requirement.

2) *TD*: As illustrated in Fig. 1(b), TD is a special case of CPD, for which the given time horizon  $[0, T]$  is divided into  $M$  equal-time slots with sufficiently short slot length  $t_m = \delta_t \triangleq T/M, m = 1, \dots, M$ . Similarly, we can apply the finite-sum approximation to the utility and constraint functions given the same finite-sum approximation accuracy as CPD. For example, the communication utility function can be approximated as

$$U(\mathbf{q}(t)) \approx \sum_{m=1}^M t_m u(\mathbf{q}_m) = \delta_t \sum_{m=1}^M u(\mathbf{q}_m) \triangleq \bar{U}_{\text{TD}}(\{\mathbf{q}_m\}). \quad (13)$$

Since each segment length should not exceed  $\Delta_{\max}$  for ensuring the desired finite-sum approximation accuracy even at the maximum UAV speed, we have  $\delta_t \leq \frac{\Delta_{\max}}{V_{\max}}$ . Thus, the number of time slots for TD,  $M$ , should satisfy  $M = \frac{T}{\delta_t} \geq \frac{TV_{\max}}{\Delta_{\max}}$ . Based on the above, with TD and the finite-sum approximation, problem (P4) can be reformulated as

$$\begin{aligned} \text{(P6)} : \quad & \max_{\{\mathbf{q}_m\}} \quad \bar{U}_{\text{TD}}(\{\mathbf{q}_m\}) \\ & \text{s.t.} \quad \bar{f}_{i,\text{TD}}(\{\mathbf{q}_m\}) \leq 0, \quad i = 1, \dots, I, \end{aligned} \quad (14a)$$

where  $\{\bar{f}_{i,\text{TD}}(\{\mathbf{q}_m\})\}$  denote the set of approximated constraints with TD.

Recall that for the CPD scheme, the time duration over each line segment can be flexibly adjusted under the constraint of  $t_n \leq \frac{\Delta_{\max}}{V_n}$  where  $V_n = \|\mathbf{v}_n\|$ . Comparing it with the time-slot length of TD (i.e.,  $\delta_t \leq \frac{\Delta_{\max}}{V_{\max}}$ ), we have  $\delta_t \leq t_n$  since  $V_n \leq V_{\max}$ , which indicates that given the same  $T$  and  $\Delta_{\max}$ ,

TD in general entails shorter time-slot length than CPD. Combining this with  $\sum_{n=1}^N t_n = M\delta_t = T$ , we conclude that TD usually requires more line segments than CPD (i.e.,  $M \geq N$ ). As shown in [1], the computational complexity for UAV trajectory and communication co-design mainly lies in the waypoint optimization. Generally speaking, the more waypoints that need to be optimized, the higher is the UAV trajectory design complexity. As such, the UAV trajectory design with CPD usually incurs less computational complexity as compared to that with TD.

### III. PROPOSED FLEXIBLE PATH DISCRETIZATION

In this section, we propose a new trajectory discretization scheme, called FPD, to reduce the UAV trajectory design complexity as compared to the existing CPD scheme in [1].

#### A. Flexible Path Discretization

Note that for the CPD scheme, the number of waypoints  $\{\mathbf{q}_n\}$  that need to be optimized may be practically large, when there is a stringent finite-sum approximation accuracy requirement (i.e., small  $\Delta_{\max}$ ) and/or the flight distance becomes long. In this case, optimizing all the  $N + 1$  waypoints for maximizing the communication utility may incur prohibitive computational complexity. To resolve this issue, a key observation is that optimizing *part* of the  $N + 1$  waypoints may not affect the finite-sum approximation accuracy (i.e., the maximum approximation error), provided that all the  $N + 1$  waypoints are employed in calculating the finite-sum approximation for the utility and constraint functions. Motivated by this, we propose a novel FPD scheme that divides the  $N + 1$  waypoints (for ensuring high finite-sum approximation accuracy) into two exclusive sets, namely, *designable* and *non-designable* waypoints, which are constructed as follows and illustrated in Fig. 1(c).

- 1) **Designable waypoints:** First, we divide the UAV path into  $L$  consecutive *long-(line)-segments* of generally unequal lengths with  $L \leq N$ . The  $L + 1$  waypoints connecting these long-segments, denoted by  $\{\mathbf{q}_\ell\}_{\ell=0}^L$ , are referred to as the designable waypoints which are used in both the (utility and constraints) function finite-sum approximation and UAV trajectory optimization. For each long-segment  $\ell \in \{1, \dots, L\}$ , we denote by  $t_\ell$  the UAV traveling time over it.
- 2) **Non-designable waypoints:** Next, given the  $L + 1$  designable waypoints  $\{\mathbf{q}_\ell\}_{\ell=0}^L$ , we further divide each long-segment, say,  $\ell$ , into  $J$  *short-(line)-segments* of *equal* length, which are characterized by the two consecutive designable waypoints at its two ends,  $\mathbf{q}_{\ell-1}$  and  $\mathbf{q}_\ell$ , as well as  $J - 1$  waypoints along the long-segment between them. These  $J - 1$  waypoints are thus called *non-designable* waypoints that are not involved in UAV trajectory optimization for reducing the design complexity, but still used in the finite-sum approximation for the utility and constraints for retaining the desired

accuracy. Mathematically, given  $\mathbf{q}_{\ell-1}$  and  $\mathbf{q}_\ell$ , the  $J - 1$  non-designable waypoints over each long-segment  $\ell$ , denoted by  $\{\mathbf{q}_\ell[j]\}_{j=1}^{J-1}$ , can be obtained as

$$\mathbf{q}_\ell[j] = \mathbf{q}_{\ell-1} + \frac{j(\mathbf{q}_\ell - \mathbf{q}_{\ell-1})}{J}, \quad j = 1, \dots, J - 1. \quad (15)$$

By assuming constant UAV speed over each short-segment, the time duration for the  $j$ -th short-segment of long-segment  $\ell$ , denoted by  $t_\ell[j]$ , is given by  $t_\ell[j] = \frac{t_\ell}{J}, j = 1, \dots, J$ .

Based on the above, the UAV trajectory under the proposed FPD scheme is represented by  $N_{\text{FPD}} \triangleq LJ$  consecutive short-segments connected by  $L + 1$  designable waypoints and  $L(J - 1)$  non-designable waypoints, as well as the time duration that the UAV spends on each of the  $L$  long-segments (or equivalently, each of its short-segments with given  $J$ ). By using the same method as in (5), the communication utility with the finite-sum approximation applied to the  $N_{\text{FPD}}$  short-segments is given by

$$\begin{aligned} U(\mathbf{q}(t)) &\approx \sum_{\ell=1}^L \left[ \left( \sum_{j=1}^{J-1} t_\ell[j] u(\mathbf{q}_\ell[j]) \right) + t_\ell[J] u(\mathbf{q}_\ell) \right] \\ &= \sum_{\ell=1}^L \left[ \frac{t_\ell}{J} \sum_{j=1}^J u \left( \mathbf{q}_{\ell-1} + \frac{j(\mathbf{q}_\ell - \mathbf{q}_{\ell-1})}{J} \right) \right] \triangleq \bar{U}_{\text{FPD}}(\{\mathbf{q}_\ell\}, \{t_\ell\}), \end{aligned} \quad (16)$$

which is determined by the designable waypoints and long-segment time durations only. Comparing (16) and (5), we observe that given the same finite-sum approximation accuracy as CPD, the short-segment length should not exceed the threshold  $\Delta_{\max}$  and hence the long-segment length should satisfy

$$\|\mathbf{q}_\ell - \mathbf{q}_{\ell-1}\| \leq J\Delta_{\max}, \quad \ell = 1, \dots, L. \quad (17)$$

As such, with the proposed FPD and finite-sum approximation, problem (P4) can be transformed into the following approximated form.

$$\begin{aligned} \text{(P7)} : \quad &\max_{\{\mathbf{q}_\ell\}, \{t_\ell\}} \bar{U}_{\text{FPD}}(\{\mathbf{q}_\ell\}, \{t_\ell\}) \\ &\text{s.t.} \quad \bar{f}_{i,\text{FPD}}(\{\mathbf{q}_\ell\}, \{t_\ell\}) \leq 0, \quad i = 1, \dots, I, \end{aligned} \quad (18a)$$

where  $\{\bar{f}_{i,\text{FPD}}(\{\mathbf{q}_\ell\}, \{t_\ell\})\}$  denote the set of approximated constraints under the FPD scheme.

Note that different from CPD for which all the  $N + 1$  waypoints required for ensuring desired finite-sum approximation accuracy are optimized for maximizing the communication utility, the proposed FPD scheme optimizes only part of the  $N + 1$  waypoints for reducing UAV trajectory design complexity, while all the  $N_{\text{FPD}} + 1 = N + 1$  (designable and non-designable) waypoints are employed in calculat-

ing the finite-sum approximation for the utility and constraints to satisfy the approximation accuracy requirements. Moreover, for the proposed FPD scheme, there exists a fundamental trade-off between UAV trajectory design complexity and communication utility performance via adjusting the number of designable waypoints,  $L + 1$ . Specifically, as  $L$  decreases, the UAV trajectory design complexity reduces due to the smaller number of designable waypoints, while the design degrees-of-freedom (DoF) for UAV trajectory also degrades since the UAV can change its flying direction and speed along the path for at most  $L - 1$  times. As such, small  $L$  may result in less optimal trajectory and thus certain utility loss as compared to that with larger  $L$ . In the special case with  $L = N$ , the proposed FPD reduces to CPD.

### B. Flexible Path Discretization versus Path/Time Discretization

In this subsection, we compare the trajectory representation of the proposed FPD scheme against the existing TD and CPD schemes.

First, the following two lemmas compare the number of waypoints required for trajectory representation between TD and CPD, as well as between CPD and FPD, respectively.

**Lemma 2.** Given  $\{T, \Delta_{\max}, V_{\max}\}$ , if the trajectory representation with TD (i.e.,  $\{\{\mathbf{q}_m\}, \delta_t\}$ ) satisfies: 1) the flying velocities over  $A_1 \geq 2$  consecutive line segments are the same, i.e.,  $\mathbf{v}_m = \mathbf{v}_{m+1} \cdots = \mathbf{v}_{m+A_1-1} = \mathbf{v}_0$  for  $1 \leq m \leq M - (A_1 + 1)$ ; and 2)  $\|\mathbf{v}_0\| \leq \frac{V_{\max}}{A_1}$ , then CPD requires  $A_1 - 1$  fewer waypoints than TD, i.e.,  $(M + 1) - (N + 1) = A_1 - 1$ .

*Proof:* Given the conditions 1) and 2), the  $A_1$  consecutive segments form a straight-line segment with a constant UAV speed  $\|\mathbf{v}_0\|$  and a total segment length satisfying  $\|\mathbf{q}_{m+A_1-1} - \mathbf{q}_{m-1}\| \leq \|\mathbf{v}_0\| A_1 \delta_t \leq \Delta_{\max}$ . Thus, these  $A_1$  segments can be regarded as one segment for CPD, represented by the two waypoints  $\{\mathbf{q}_{m-1}, \mathbf{q}_{m+A_1-1}\}$ , together with a UAV traveling duration  $A_1 \delta_t$ . Hence,  $K + 1 - 2 = K - 1$  waypoints are saved for trajectory representation.  $\square$

**Lemma 3.** Given  $\{T, \Delta_{\max}, V_{\max}\}$ , if the trajectory representation with CPD (i.e.,  $\{\{\mathbf{q}_n\}, \{t_n\}\}$ ) satisfies that the flying velocities over  $A_2 \geq 2$  consecutive line segments are the same, i.e.,  $\mathbf{v}_n = \mathbf{v}_{n+1} \cdots = \mathbf{v}_{n+A_2-1}$  for  $1 \leq n \leq N - (A_2 + 1)$ , then the proposed FPD requires  $A_2 - 1$  fewer designable waypoints than CPD, i.e.,  $(N + 1) - (L + 1) = A_2 - 1$ .

Lemma 3 can be proved by using the similar method as for proving Lemma 2, thus the details are omitted for brevity.

Lemma 2 indicates that if the UAV hovers or moves slowly at the same direction and speed, CPD requires fewer (designable) waypoints than TD. Moreover, Lemma 3 shows that compared to CPD,

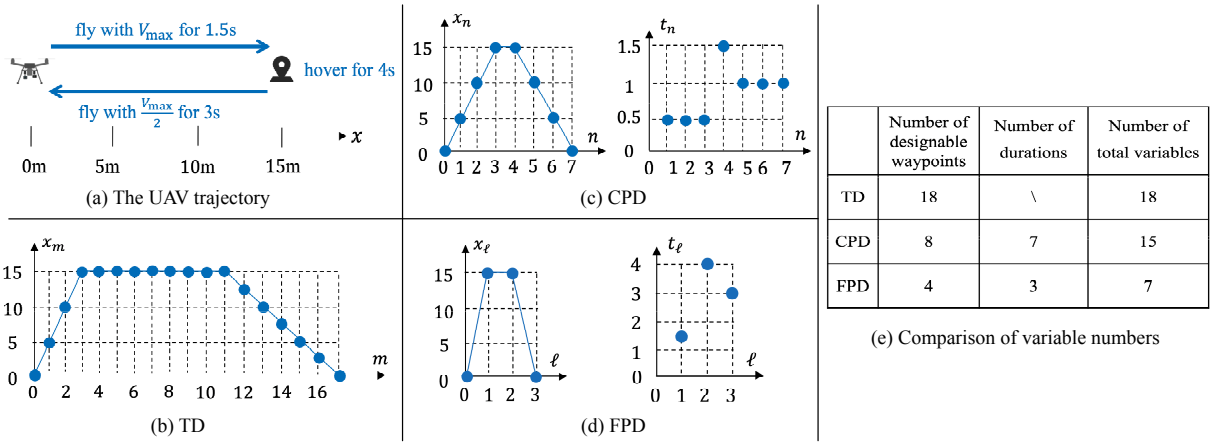


Fig. 2: Trajectory representation under different trajectory discretization schemes.

FPD in general can represent the UAV trajectory with even fewer (designable) waypoints as long as the UAV flies at the same velocity along (part of) its path, even at the maximum speed. For example, in the extreme case where the UAV flies at a constant velocity towards the destination, FPD requires only 2 designable waypoints (i.e., start and end locations) as well as its traveling duration for characterizing the trajectory, which in general is much smaller than that of CPD with  $N+1 = \left\lceil \frac{\|\mathbf{q}_{\text{str}} - \mathbf{q}_{\text{end}}\|}{\Delta_{\text{max}}} \right\rceil + 1$  waypoints. For ease of illustration, a concrete example is provided below for comparing the number of waypoints/time durations/design variables required for trajectory representation under different trajectory discretization schemes.

**Example 2.** Consider an example illustrated in Fig. 2(a), where the UAV flies along the  $x$ -axis. The 1D UAV trajectory consists of three consecutive phases: 1) the UAV flies from  $x = 0$  m to  $x = 15$  m at the maximum speed of  $V_{\text{max}} = 10$  m/s with a flight duration of 1.5 s; 2) it hovers above  $x = 15$  m for 4 s; 3) the UAV flies back to  $x = 0$  m at a constant speed of  $\frac{V_{\text{max}}}{2} = 5$  m/s with a flight duration of 3 s. We set  $\Delta_{\text{max}} = 5$  m and have the following main observations. First, for TD, we have  $\delta_t = \frac{\Delta_{\text{max}}}{V_{\text{max}}} = 0.5$  s and the total flight period  $T = 8.5$  s. Hence, TD requires  $8.5/0.5 + 1 = 18$  waypoints in total for trajectory representation, as shown in Fig. 2(b). Second, for CPD, it requires only 2 waypoints plus the hovering time duration to represent phase 2 of UAV's hovering and 3 waypoints for phase 3 with the UAV flying at a low speed; thus it involves 8 waypoints and 7 time durations in total as shown in Fig. 2(c). Last, for the proposed FPD with  $J = 3$ , both phases 1 and 3 can be characterized by a long-segment with its corresponding flight duration since the UAV flies at a constant velocity. As such, 4 designable waypoints and 3 time durations are sufficient for the trajectory representation, as shown in Fig. 2(d). In summary, the numbers of required design variables under different trajectory discretization schemes are compared in Fig. 2(e).

#### IV. PROPOSED PATH COMPRESSION

The FPD scheme proposed in the preceding section reduces the UAV trajectory design complexity in the *time* domain via reducing the number of designable waypoints. In this section, we propose another alternative approach, called *path compression*, to further reduce the UAV trajectory design variables in the *spatial* domain.

##### A. Path Decomposition

Without loss of generality, we consider the UAV path with FPD introduced in Section III as it includes TD and CPD as special cases, while the results can also be extended to other trajectory discretization schemes. Recall that with FPD, the UAV piecewise-linear trajectory can be characterized by the pre-determined parameters  $\{L, J\}$ , the designable waypoints  $\{\mathbf{q}_\ell\}$ , as well as the corresponding time durations  $\{t_\ell\}$ . For this *waypoint-based* path representation, the UAV path  $\{\mathbf{q}_\ell\}$  is decomposed into  $L + 1$  waypoints and each waypoint  $\mathbf{q}_\ell = [q_{\ell,x}, q_{\ell,y}, q_{\ell,z}]^T$  is represented in the 3D Cartesian coordinate system. Thereby, the UAV trajectory is completely represented by  $3(L + 1)$  waypoint variables and  $L$  time variables. In this subsection, we propose a new *sub-path-based* path representation, for which the 3D UAV path  $\{\mathbf{q}_\ell\}$  is decomposed into three 1D sub-paths in each of the 3D Cartesian coordinates, namely,  $\{\mathbf{q}_\ell\}_{\ell=0}^L = \{\mathbf{q}_x, \mathbf{q}_y, \mathbf{q}_z\}$  where  $\mathbf{q}_{\text{dim}} = [q_{0,\text{dim}}, \dots, q_{L,\text{dim}}]^T \in \mathbb{R}^{(L+1) \times 1}$  for  $\text{dim} = x, y, z$ . Then, by constructing  $L + 1$  *basis paths* (or so-called *path features*), we are able to represent each sub-path by a superposition of the  $L + 1$  basis paths with flexibly chosen combining weights. For simplicity, we consider in this paper that a common set of basis paths are used for each of the three sub-paths in 3D, while the results can be extended to the general case with different basis paths for different sub-paths.

Define  $\{\mathbf{p}_\ell\}_{\ell=0}^L$  as a set of basis paths with  $\mathbf{p}_\ell \in \mathbb{R}^{(L+1) \times 1}, \ell = 0, \dots, L$ , provided that  $\mathbf{p}_\ell$ 's are linearly independent (as will be exemplified later). With  $\{\mathbf{p}_\ell\}_{\ell=0}^L$ , the three sub-paths can be equivalently represented by

$$(\mathbf{q}_{\text{dim}})^T = \sum_{\ell=0}^L c_{\ell,\text{dim}} \mathbf{p}_\ell^T = (\mathbf{c}_{\text{dim}})^T \mathbf{P}, \quad \text{dim} = x, y, z, \quad (19)$$

where  $\mathbf{c}_{\text{dim}} = [c_{0,\text{dim}}, \dots, c_{L,\text{dim}}]^T \in \mathbb{R}^{(L+1) \times 1}$  with  $c_{\ell,\text{dim}}$  denoting the path coefficient for basis path  $\ell$  in the specified dimension, and  $\mathbf{P} \triangleq [\mathbf{p}_0, \dots, \mathbf{p}_L]^T \in \mathbb{R}^{(L+1) \times (L+1)}$  is named as the *basis-path matrix*. Let  $\mathbf{Q} = [\mathbf{q}_0, \dots, \mathbf{q}_L] = [\mathbf{q}_x, \mathbf{q}_y, \mathbf{q}_z]^T \in \mathbb{R}^{3 \times (L+1)}$  denote the *waypoint-matrix* that stacks all the  $L + 1$  designable waypoints. Based on the above,  $\mathbf{Q}$  can be expressed in the following compact form

$$\mathbf{Q} = \mathbf{C}\mathbf{P}, \quad (20)$$

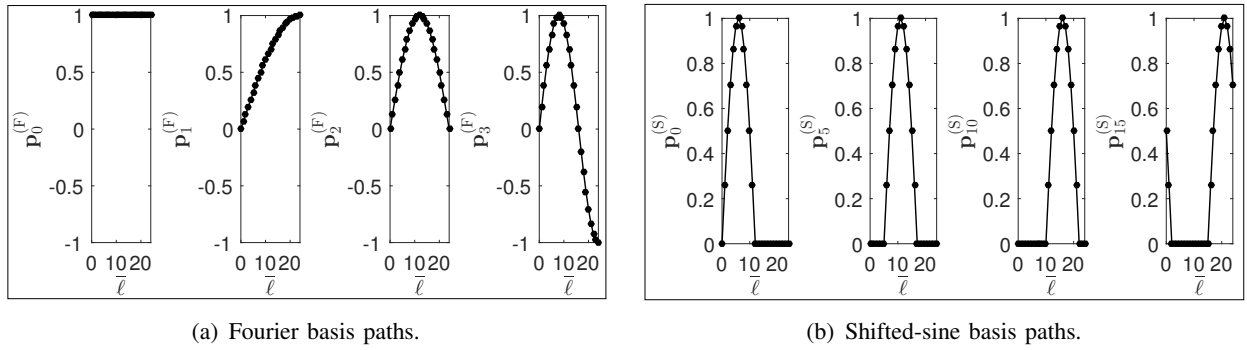


Fig. 3: Two example types of basis paths.

where  $\mathbf{C} = [\mathbf{c}_x, \mathbf{c}_y, \mathbf{c}_z]^T \in \mathbb{R}^{3 \times (L+1)}$  denotes the *path-coefficient* matrix. Since the basis paths are linearly independent,  $\mathbf{P}$  is of full-rank and thus we have  $\mathbf{C} = \mathbf{Q}\mathbf{P}^{-1}$ . This means that under the new path coordinate system  $\mathbf{P}$ , the 3D UAV path  $\mathbf{Q}$  can be fully characterized by the path-coefficient matrix  $\mathbf{C}$  with  $3(L+1)$  variables that flexibly weight the basis paths for constructing a desired path.

In general, there are various types of basis paths for  $\mathbf{P}$ , provided that they satisfy  $\text{rank}(\mathbf{P}) = L+1$ . In the following, we propose two example types of basis paths.

**Example 3** (Fourier basis paths). Inspired by the Fourier decomposition for the continuous function, we define the Fourier basis paths as  $\mathbf{p}_\ell^{(F)} = [p_{\ell,0}^{(F)}, \dots, p_{\ell,L}^{(F)}]$  for  $\ell = 0, \dots, L$ , where

$$p_{\ell,\tilde{\ell}}^{(F)} = \begin{cases} \sin\left(\frac{\pi\ell\tilde{\ell}}{2L}\right), & \tilde{\ell} = 0, \dots, L, \quad \ell = 1, \dots, L, \\ 1, & \text{otherwise,} \end{cases} \quad (21)$$

Fig. 3(a) depicts some of the above defined Fourier basis paths for the case with  $L = 24$ . It is observed that the basis-path variation over  $\tilde{\ell}$  (or *path frequency*) increases with the sub-path index  $\ell$ . Thus, one can draw an analogy between the path frequency and Fourier series, where the higher-order basis path corresponds to “higher-frequency” component in each sub-path.

**Example 4** (Shifted-sine basis paths). The shifted-sine basis paths are defined as  $\mathbf{p}_\ell^{(S)} = [p_{\ell,0}^{(S)}, \dots, p_{\ell,L}^{(S)}]$  for  $\ell = 0, \dots, L$ , where

$$p_{\ell,\tilde{\ell}}^{(S)} = \begin{cases} \sin\left(\frac{2\pi(\tilde{\ell}-\ell)}{L}\right), & \tilde{\ell} \in [0, b_1(\ell)] \cup [\ell, b_2(\ell)], \quad \ell = 0, \dots, L, \\ 0, & \text{otherwise,} \end{cases} \quad (22)$$

with  $b_1(\ell) = \max\{0, \ell - \frac{L}{2} - 1\}$  and  $b_2(\ell) = \min\{\frac{L}{2} + \ell, L\}$ . Fig. 3(b) plots some of the defined shifted-sine basis paths for the case with  $L = 24$ . One can observe that the basis paths for different  $\ell \geq 1$  are shifted versions of  $\mathbf{p}_0^{(S)}$  and thus they have similar shapes.



## B. Path Compression

Based on the Fourier basis paths proposed in the previous subsection as an example, we propose in this subsection a simple yet efficient method, named PC, to compress the UAV path in the spatial domain and then reformulate the UAV trajectory optimization problem based on PC. Note that the proposed PC method can be similarly applied to other basis paths (e.g., shifted-sine basis paths in Example 4).

The main idea of PC is to approximate the UAV path as a superposition of some selected Fourier basis paths only but still retain the main desired features of the path, thus achieving lower path design complexity yet with tolerable path-compression error. To be specific, let  $K$  with  $0 < K \leq L + 1$  denote the number of selected Fourier basis paths among the full  $L + 1$  basis paths (which fully characterize the  $L + 1$  waypoints). We define  $\rho_{\text{comp}} = \frac{K}{L+1} \in (0, 1]$  as the path-compression ratio. Since the UAV path is usually preferred to be smooth in practice, we select the first  $K$  basis paths that have relatively low path frequencies to construct a reduced-dimensional basis-path matrix  $\bar{\mathbf{P}} \triangleq [\bar{\mathbf{p}}_0, \dots, \bar{\mathbf{p}}_{K-1}]^T \in \mathbb{R}^{K \times (L+1)}$ . Then, the UAV path can be approximately characterized by the following compressed path-coefficient matrix  $\bar{\mathbf{C}}$

$$\mathbf{Q} \approx \bar{\mathbf{Q}} \triangleq \bar{\mathbf{C}}\bar{\mathbf{P}}, \quad (23)$$

where  $\bar{\mathbf{C}} = [\bar{\mathbf{c}}_x, \bar{\mathbf{c}}_y, \bar{\mathbf{c}}_z]^T \in \mathbb{R}^{3 \times K}$  with  $\bar{\mathbf{c}}_{\text{dim}} = [c_{0,\text{dim}}, \dots, c_{K-1,\text{dim}}]^T \in \mathbb{R}^{K \times 1}$ ,  $\text{dim} = x, y, z$  denoting the compressed path coefficient vector for the sub-path in each corresponding dimension. Note that there exists a fundamental trade-off between the PC ratio (or path design complexity) and compression accuracy (or communication performance). Intuitively, as  $K$  decreases, although fewer basis paths are selected which leads to a smaller number of path coefficients to be optimized, it also results in less DoF in optimizing the UAV path that may cause communication performance degradation.

In Fig. 4, we numerically compare the compressed path by the proposed Fourier-based PC with different  $K$  against the benchmark scheme based on the shifted-sine basis paths introduced in Example 4. First, it is observed that for the proposed Fourier-based PC, as  $K$  increases, the approximated UAV path gets closer to the actual path with more path basis components selected. Second, it is interesting to observe that for the path with  $L + 1 = 25$  waypoints, the proposed Fourier-based PC with small  $K$  (e.g.,  $K = 5$ ) achieves very close path approximation performance as that with large  $K$  (e.g.,  $K = 24$ ). This can be explained by the fact that the basis paths with low-order path frequencies contain most of information for this smooth path in practice. Thus, discarding high-frequency basis paths does not compromise the approximation accuracy notably. Third, the proposed Fourier-based PC significantly outperforms the benchmark scheme based on the shifted-sine basis paths for different  $K$ , since the

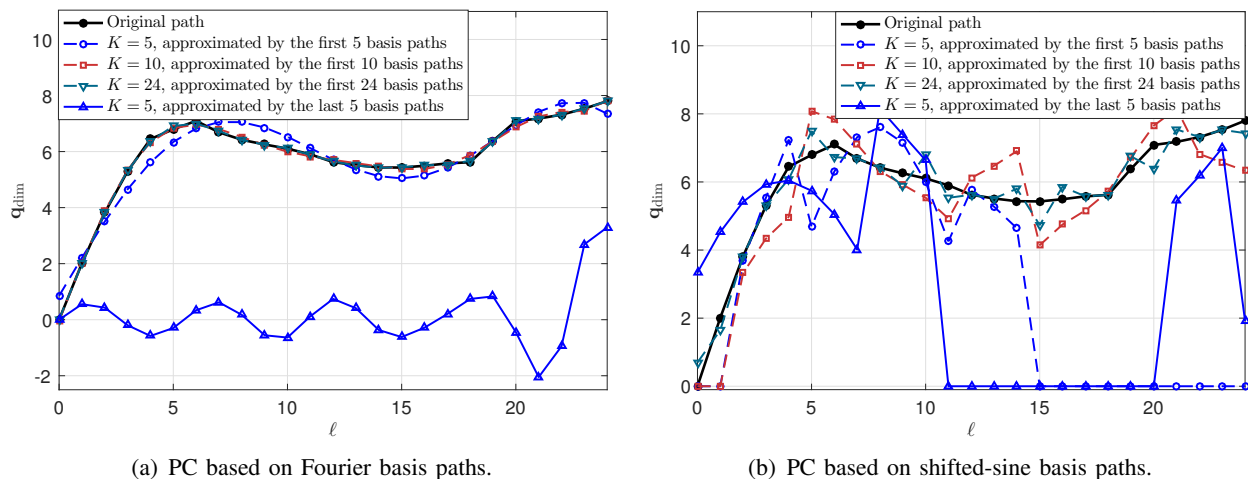


Fig. 4: Comparison of path approximation for PC based on different basis paths.

basis paths of the latter scheme are equally important and thus the approximation accuracy is very sensitive to the number of (shifted) basis paths selected.

With the proposed Fourier-based PC, the designable waypoints with FPD can be rewritten as  $\mathbf{q}_\ell = \bar{\mathbf{C}}[\bar{\mathbf{P}}]_{:, \ell+1}$ , where  $[\bar{\mathbf{P}}]_{:, \ell+1}$  denotes the  $(\ell + 1)$ -th column of  $\bar{\mathbf{P}}$ . Thus, the communication utility function for the combined FPD with PC (termed FPD-PC) is given by

$$\bar{U}_{\text{FPD-PC}}(\bar{\mathbf{C}}, \{t_\ell\}) = \bar{U}_{\text{FPD}}(\{\bar{\mathbf{C}}[\bar{\mathbf{P}}]_{:, \ell+1}\}, \{t_\ell\}), \quad (24)$$

where the function  $\bar{U}_{\text{FPD}}(\cdot)$  is defined in (16). As such, problem (P4) can be approximated by

$$\begin{aligned} \text{(P8)} : \quad & \max_{\bar{\mathbf{C}}, \{t_\ell\}} \bar{U}_{\text{FPD-PC}}(\bar{\mathbf{C}}, \{t_\ell\}) \\ \text{s.t.} \quad & \bar{f}_{i, \text{FPD-PC}}(\bar{\mathbf{C}}, \{t_\ell\}) \leq 0, \quad i = 1, \dots, I, \end{aligned} \quad (25a)$$

where  $\{\bar{f}_{i, \text{FPD-PC}}(\bar{\mathbf{C}}, \{t_\ell\})\}$  denote the set of approximated constraints. Note that compared to the FPD scheme without PC in Section III that requires  $3(L + 1) + L$  design variables, the new FPD-PC scheme has reduced the number of path design variables to  $3K + L$  with  $K \leq L + 1$ .

## V. CASE STUDY: UAV TRAJECTORY DESIGN FOR MIN-RATE MAXIMIZATION

A case study is provided in this section to show different formulations of the same min-rate maximization problem under different trajectory discretization schemes with/without PC. Their computational complexities for solving their respective optimization problems are analyzed as well.

Similar to Example 1, we consider a UAV-enabled data harvesting system where a UAV is dispatched to collect data from  $S$  ground SNs, denoted by the set  $\mathcal{S} = \{1, \dots, S\}$ . Let  $\mathbf{w}_s \in \mathbb{R}^{3 \times 1}$ ,  $s \in \mathcal{S}$  denote

the location of SN  $s$  and we assume that the UAV starts its flight from  $\mathbf{q}_{\text{str}}$  and flies back to  $\mathbf{q}_{\text{end}} = \mathbf{q}_{\text{str}}$  after a flight period of  $T$ . For the purpose of exposition, we consider the LoS UAV-ground channel model [1], while the results can be extended to the more general UAV-ground channel models (e.g., the elevation-angle dependent Rician fading channel [10] and probabilistic LoS channel [11]). Under this channel model, the UAV is assumed to fly at a fixed minimum UAV altitude  $H_{\text{min}}$ . Moreover, we consider time division multiple access (TDMA) for the UAV communication scheduling and denote by  $\alpha_s(t) \in \{0, 1\}$  the association variable for user  $s$  at time  $t$ , where  $\alpha_s(t) = 1$  indicates that SN  $s$  is scheduled by the UAV for transmission and otherwise it keeps silent. As such, the average data collection rate of the UAV from SN  $s$  is given by

$$R_s = \frac{1}{T} \int_0^T \alpha_s(t) \log_2 \left( 1 + \frac{P_s \beta_0}{\|\mathbf{q}(t) - \mathbf{w}_s\|^2 \sigma^2} \right) dt, \quad (26)$$

where  $P_s$  denotes the transmit power of SN  $s$ , and  $\{\beta_0, \sigma^2\}$  are defined in Example 1.

Our objective is to maximize the minimum (average) achievable rate among all the  $S$  ground SNs by jointly designing the UAV continuous-time piecewise-linear trajectory and communication scheduling, i.e.,  $U(\mathcal{Q}(t), \mathcal{R}(t)) = \min_{s \in \mathcal{S}} R_s$ , where  $\mathcal{Q}(t) = \mathbf{q}(t)$  and  $\mathcal{R}(t) = \{\alpha_s(t)\}_{s=1}^S$  in (P1). Under the practical constraints on the UAV trajectory and communication scheduling, the above min-rate maximization problem is formulated as

$$\begin{aligned} \text{(P9)} : \quad & \max_{\mathbf{q}(t), \{\alpha_s(t)\}} \quad \min_{s \in \mathcal{S}} R_s \\ \text{s.t.} \quad & \|\dot{\mathbf{q}}(t)\| \leq V_{\text{max}}, \quad q_z(t) = H_{\text{min}}, \quad \forall t \in [0, T], \end{aligned} \quad (27a)$$

$$\mathbf{q}(0) = \mathbf{q}_{\text{str}}, \quad \mathbf{q}(T) = \mathbf{q}_{\text{end}}, \quad (27b)$$

$$\sum_{s=1}^S \alpha_s(t) \leq 1, \quad \forall t \in [0, T], \quad (27c)$$

$$\alpha_s(t) \in \{0, 1\}, \quad \forall s \in \mathcal{S}, \quad t \in [0, T], \quad (27d)$$

where (27a) imposes the constraints on the UAV maximum speed and fixed altitude, (27b) specifies the UAV start/end locations, (27c) restricts the UAV scheduling with one user only at each time instant, and (27d) denotes the binary communication scheduling constraint for  $\alpha_s(t)$  over  $t$ .

### A. Problem Reformulation

1) *TD*: For the TD scheme, we set  $\delta_t = \Delta_{\text{max}}/V_{\text{max}}$  given a properly chosen  $\Delta_{\text{max}}$  and thus  $M = T/\delta_t$  (assumed to be an integer). Similar to [7], the binary communication scheduling constraint for each

time slot  $m$  in (27d) is relaxed as  $0 \leq \alpha_{s,m} \leq 1, \forall s \in \mathcal{S}, m = 1, \dots, M$ . Then the approximated communication utility under the TD scheme is given by  $\bar{U}_{\text{TD}}(\{\mathbf{q}_m\}, \{\alpha_{s,m}\}) = \min_{s \in \mathcal{S}} \bar{R}_{s,\text{TD}}$ , where  $\bar{R}_{s,\text{TD}} = \frac{1}{M} \sum_{m=1}^M \alpha_{s,m} \log_2 \left( 1 + \frac{P_s \beta_0}{\|\mathbf{q}_m - \mathbf{w}_s\|^2 \sigma^2} \right)$ . As such, with TD, problem (P9) is reformulated as

$$(P10) : \quad \max_{\{\mathbf{q}_m\}, \{\alpha_{s,m}\}} \quad \min_{s \in \mathcal{S}} \bar{R}_{s,\text{TD}} \quad (28a)$$

$$\text{s.t.} \quad \|\mathbf{q}_m - \mathbf{q}_{m-1}\| \leq \Delta_{\max}, \quad m = 1, \dots, M, \quad (28a)$$

$$\mathbf{q}_0 = \mathbf{q}_{\text{str}}, \quad \mathbf{q}_M = \mathbf{q}_{\text{end}}, \quad q_{m,z} = H_{\min}, \quad m = 0, \dots, M, \quad (28b)$$

$$\sum_{s=1}^S \alpha_{s,m} \leq 1, \quad 0 \leq \alpha_{s,m} \leq 1, \quad \forall s \in \mathcal{S}, \quad m = 1, \dots, M. \quad (28c)$$

Note that given fixed UAV altitude, we only need to optimize the 2D horizontal trajectory for  $\{\mathbf{q}_m\}$ .

2) *CPD*: With CPD and given the same  $\Delta_{\max}$  as for TD, the UAV trajectory can be characterized by  $\{\{\mathbf{q}_n\}_{n=0}^N, \{t_n\}_{n=1}^N\}$ . Following the procedures in Section II-B, the communication utility function can be approximated by  $\bar{U}_{\text{CPD}}(\{\mathbf{q}_n\}, \{t_n\}, \{\alpha_{s,n}\}) = \min_{s \in \mathcal{S}} \bar{R}_{s,\text{CPD}}$ , where  $\bar{R}_{s,\text{CPD}} = \frac{1}{T} \sum_{n=1}^N \alpha_{s,n} t_n \log_2 \left( 1 + \frac{P_s \beta_0}{\|\mathbf{q}_n - \mathbf{w}_s\|^2 \sigma^2} \right)$ . As such, problem (P9) can be approximately reformulated as

$$(P11) : \quad \max_{\{\mathbf{q}_n\}, \{t_n\}, \{\alpha_{s,n}\}} \quad \min_{s \in \mathcal{S}} \bar{R}_{s,\text{CPD}} \quad (29a)$$

$$\text{s.t.} \quad \|\mathbf{q}_n - \mathbf{q}_{n-1}\| \leq \min\{\Delta_{\max}, t_n V_{\max}\}, \quad n = 1, \dots, N, \quad (29a)$$

$$\mathbf{q}_0 = \mathbf{q}_{\text{str}}, \quad \mathbf{q}_N = \mathbf{q}_{\text{end}}, \quad q_{n,z} = H_{\min}, \quad n = 0, \dots, N, \quad (29b)$$

$$\sum_{s=1}^S \alpha_{s,n} \leq 1, \quad 0 \leq \alpha_{s,n} \leq 1, \quad \forall s \in \mathcal{S}, \quad n = 1, \dots, N, \quad (29c)$$

$$\sum_{n=1}^N t_n \leq T, \quad n = 1, \dots, N. \quad (29d)$$

3) *FPD*: Note that for the proposed FPD scheme with parameter  $\{L, J\}$ , the time duration of the  $j$ -th short-segment of long-segment  $\ell$  (i.e.,  $t_\ell/J$ ) is shared by all the users. Thus, the approximated communication utility is given by  $\bar{U}_{\text{FPD}}(\{\mathbf{q}_\ell\}, \{t_\ell\}, \{\alpha_{s,\ell}[j]\}) = \min_{s \in \mathcal{S}} \bar{R}_{s,\text{FPD}}$ , where  $\bar{R}_{s,\text{FPD}} = \frac{1}{T} \sum_{\ell=1}^L \sum_{j=1}^J \alpha_{s,\ell}[j] \frac{t_\ell}{J} \log_2 \left( 1 + \frac{P_s \beta_0}{\|\mathbf{q}_\ell[j] - \mathbf{w}_s\|^2 \sigma^2} \right)$  with  $\mathbf{q}_\ell[j] = \mathbf{q}_\ell + \frac{j(\mathbf{q}_\ell - \mathbf{q}_{\ell-1})}{J}$  and  $\alpha_{s,\ell}[j]$  denoting the communication scheduling variable of user  $s$  at the  $j$ -th short-segment of long-segment  $\ell$ . As such, with FPD, problem (P9) can be approximately formulated as

$$(P12) : \quad \max_{\{\mathbf{q}_\ell\}, \{t_\ell\}, \{\alpha_{s,\ell}[j]\}} \quad \min_{s \in \mathcal{S}} \bar{R}_{s,\text{FPD}} \quad (30a)$$

$$\text{s.t.} \quad \|\mathbf{q}_\ell - \mathbf{q}_{\ell-1}\| \leq \min\{J \Delta_{\max}, t_\ell V_{\max}\}, \quad \ell = 1, \dots, L, \quad (30a)$$

$$\mathbf{q}_0 = \mathbf{q}_{\text{str}}, \mathbf{q}_L = \mathbf{q}_{\text{end}}, q_{\ell,z} = H_{\min}, \ell = 0, \dots, L, \quad (30b)$$

$$\sum_{s=1}^S \alpha_{s,\ell}[j] \leq 1, 0 \leq \alpha_{s,\ell}[j] \leq 1, \forall s \in \mathcal{S}, j = 1, \dots, J, \ell = 1, \dots, L, \quad (30c)$$

$$\sum_{\ell=1}^L t_\ell \leq T, \ell = 1, \dots, L. \quad (30d)$$

4) *FPD-PC*: Recall that for PC, we construct the reduced basis-path matrix  $\bar{\mathbf{P}}$  based on the first  $K$  Fourier basis paths in (21) and the designable waypoints are functions of the reduced path coefficients, i.e.,  $\mathbf{q}_\ell = \bar{\mathbf{C}}[\bar{\mathbf{P}}]_{:, \ell+1}, \ell = 0, \dots, L$ . Thus, the approximated communication utility is given by  $\bar{U}_{\text{FPD-PC}}(\bar{\mathbf{C}}, \{t_\ell\}, \{\alpha_{s,\ell}[j]\}) = \min_{s \in \mathcal{S}} \bar{R}_{s,\text{FPD-PC}}$ , where  $\bar{R}_{s,\text{FPD-PC}}$  has a similar form as  $\bar{R}_{s,\text{FPD}}$  but with  $\mathbf{q}_\ell$  replaced by  $\bar{\mathbf{C}}[\bar{\mathbf{P}}]_{:, \ell+1}$ . Note that given fixed UAV altitude  $H_{\min}$ , we only need to optimize the UAV horizontal trajectory and thus only the first two rows of the compressed coefficient matrix, i.e.,  $[\bar{\mathbf{C}}]_{1:2,:}$ . As such, problem (P9) is approximated by

$$\begin{aligned} \text{(P13)} : \quad & \max_{[\bar{\mathbf{C}}]_{1:2,:}, \{t_\ell\}, \{\alpha_{s,\ell}[j]\}} \min_{s \in \mathcal{S}} \bar{R}_{s,\text{FPD-PC}} \\ & \text{s.t.} \quad \|[ [\bar{\mathbf{C}}]_{1:2,:} [\bar{\mathbf{P}}]_{:, \ell+1} - [\bar{\mathbf{C}}]_{1:2,:} [\bar{\mathbf{P}}]_{:, \ell} ]\| \leq \min\{J\Delta_{\max}, t_\ell V_{\max}\}, \ell = 1, \dots, L, \end{aligned} \quad (31a)$$

$$[\bar{\mathbf{C}}]_{1:2,:} [\bar{\mathbf{P}}]_{:,1} = [\mathbf{q}_{\text{str}}]_{1:2}, \quad [\bar{\mathbf{C}}]_{1:2,:} [\bar{\mathbf{P}}]_{:,L+1} = [\mathbf{q}_{\text{end}}]_{1:2}, \quad (31b)$$

(30c) – (30d).

Problems (P10)–(P13) are non-convex optimization problems due to the coupling among the 2D UAV waypoints, traveling durations on line segments, as well as UAV communication scheduling. To tackle this difficulty, we can use the BCD method to decouple the variables into multiple blocks. For example, for the case with FPD, problem (P12) can be decomposed into three subproblems, corresponding to the optimization for the blocks of  $\{\mathbf{q}_\ell\}$ ,  $\{t_\ell\}$ , and  $\{\alpha_{s,\ell}[j]\}$ , respectively. Although the subproblems associated with  $\{t_\ell\}$  and  $\{\alpha_{s,\ell}[j]\}$  can be optimally solved owing to their convexity, the optimization problem for  $\{\mathbf{q}_\ell\}$  in general is still non-convex and thus difficult to solve. Fortunately, it has been shown in the existing literature (see, e.g., [1]) that the SCA technique can be utilized to transform this kind of non-convex optimization problem into solving a series of relaxed convex optimization problems so as to obtain its suboptimal solution efficiently. The details are thus omitted for brevity.

## B. Proposed Algorithms and Complexity Analysis

Instead, we focus on analyzing the computational complexity of the algorithms based on the BCD and SCA with different UAV trajectory discretization schemes. Specifically, the 2D trajectory (or

Optimization problem	Trajectory design		Communication design	
	$N_{\text{trj}}$	Complexity order	$N_{\text{com}}$	Complexity order
(P10): TD	$2(M + 1)$	$\mathcal{O}(M^{3.5} \log(1/\epsilon))$	$UM$	$\mathcal{O}((UM)^{3.5} \log(1/\epsilon))$
(P11): CPD	$2(N + 1)$	$\mathcal{O}(N^{3.5} \log(1/\epsilon))$	$UN + N$	$\mathcal{O}((UN + N)^{3.5} \log(1/\epsilon))$
(P12): FPD	$2(L + 1)$	$\mathcal{O}(L^{3.5} \log(1/\epsilon))$	$ULJ + L$	$\mathcal{O}((ULJ + L)^{3.5} \log(1/\epsilon))$
(P13): FPD-PC	$2K$	$\mathcal{O}(K^{3.5} \log(1/\epsilon))$	$ULJ + L$	$\mathcal{O}((ULJ + L)^{3.5} \log(1/\epsilon))$

Table II: Comparison of computational complexities of different trajectory discretization schemes with/without PC. Note that  $K \leq L \leq N \leq M$  in general.

waypoints) optimization can be solved by the standard interior-point method with the complexity order of  $\mathcal{O}(N_{\text{trj}}^{3.5} \log(1/\epsilon))$  [28], where  $N_{\text{trj}}$  denotes the number of scalar variables for trajectory optimization and  $\epsilon > 0$  is the solution accuracy. On the other hand, the communication design problem is an LP in our considered problem and has the (worst-case) complexity order of  $\mathcal{O}(N_{\text{com}}^{3.5} \log(1/\epsilon))$  [28], where  $N_{\text{com}}$  denotes the number of variables relevant to the communication design. Notice that although the trajectory design has the same complexity scaling order as the communication counterpart in terms of number of scalar variables, it involves solving a second-order cone programming (SOCP) which usually takes much longer running time than solving an LP for the communication design by using well-known optimization softwares e.g., CVX [29]; as such, their total complexity is generally dominated by the trajectory design, when the number of variables for both designs are practically large. Based on the above, we summarize in Table II the computational complexity required for solving problems (P10)–(P13) with TD, CPD, FPD, and FPD-PC, respectively. It is observed that the UAV trajectory and communication co-design with the proposed FPD scheme has lower total complexity as compared to TD and CPD, while the proposed FPD-PC scheme further reduces the complexity of FPD (without PC). The communication performance of these UAV trajectory designs will be evaluated in the next section by simulation.

## VI. NUMERICAL RESULTS

Numerical results are presented in this section to verify the effectiveness of the proposed FPD and PC schemes. We consider a UAV-enabled data harvesting system with 10 ground SNs randomly and uniformly distributed in a square area of  $100 \times 100 \text{ m}^2$ . For ease of illustration, the following results are based on one specific realization of SNs' locations. The UAV starts its flight from the location  $\mathbf{q}_{\text{str}} = [0, 0, 100]^T$  and flies back to  $\mathbf{q}_{\text{end}} = \mathbf{q}_{\text{str}}$  after a flight period of  $T = 100 \text{ s}$ , given a fixed (minimum) UAV flight altitude of  $H_{\text{min}} = 100 \text{ m}$  and maximum UAV (horizontal) speed of  $V_{\text{max}} = 20 \text{ m/s}$ . The tolerable finite-sum approximation error for the communication utility is set as  $E_u = 0.05$

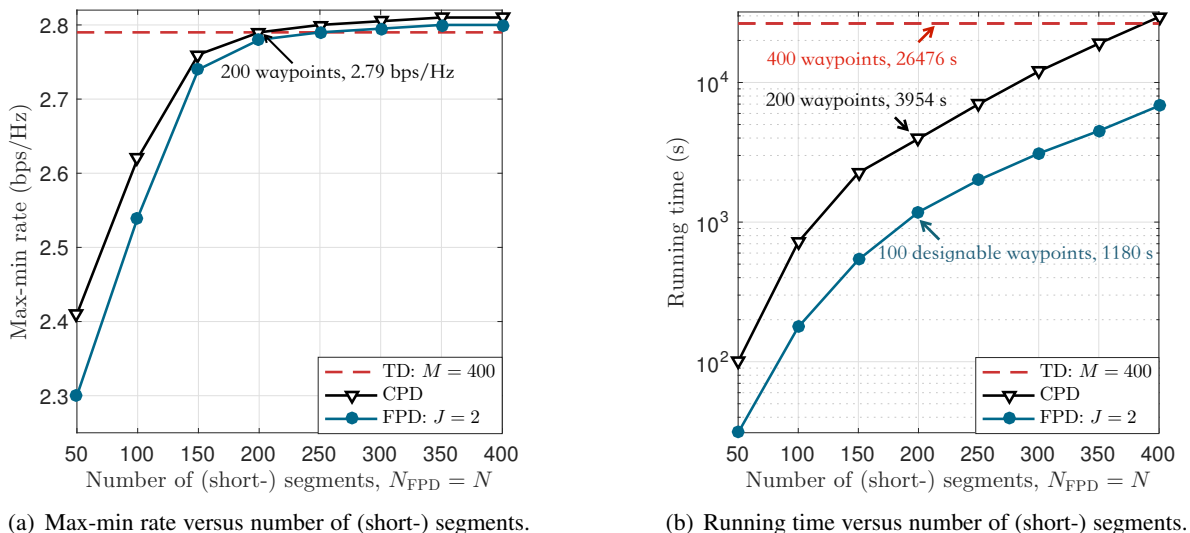


Fig. 5: Performance comparison of different trajectory discretization schemes.

bps/Hz. As such, we obtain  $\Delta_{\max} \leq 5.41$  m from Lemma 1 and hence set  $\Delta_{\max} = 5$  m for simplicity. For TD, the time-slot length is obtained as  $\delta_t = \Delta_{\max}/V_{\max} = 0.25$  s and the number of time slots is  $M = T/\delta_t = 400$ . Moreover, the channel power gain at the reference distance of 1 m is set as  $\beta_0 = -60$  dB, the receiver noise power is  $\sigma^2 = -90$  dBW, and all the SNs' are assumed to send data at the same transmit power  $P_s = 0.2$  W,  $\forall s \in \mathcal{S}$ . All simulations are run in MATLAB 2016b, which operates on a computer equipped with Intel-i7, 3.5 Hz processor, and 16 GB RAM memory.

#### A. Performance of Proposed Flexible Path Discretization

In Figs. 5(a) and 5(b), we compare the achievable max-min rate and algorithm running time by the proposed FPD scheme with  $J = 2$  (i.e., 2 short-segments in each long-segment) versus its number of short-segments,  $N_{\text{FPD}}$ , against the TD and CPD benchmark schemes. Notice that for comparison, the horizontal axis represents the number of segments for the CPD benchmark ( $N$ ) as well. The main observations are given as follows. First, it is observed that as  $N_{\text{FPD}}$  increases, the max-min rate of the proposed FPD scheme firstly grows fast and then saturates after  $N_{\text{FPD}}$  exceeds a certain threshold (see Fig. 5(a)), while its running time monotonically increases with  $N_{\text{FPD}}$ . The diminishing rate improvement with  $N_{\text{FPD}}$  can be explained by the fact that increasing the number of designable waypoints significantly improves the UAV trajectory design when  $N_{\text{FPD}}$  is small, while the improvement becomes marginal when  $N_{\text{FPD}}$  is relatively large as it only results in small trajectory adjustment. The same rate and running time trends apply to the CPD scheme as well since it can be regarded as a special case of the FPD scheme with  $J = 1$ . Second, comparing the three trajectory discretization schemes, one can observe that the CPD scheme achieves smaller max-min rate than the TD scheme when  $N$  is small,

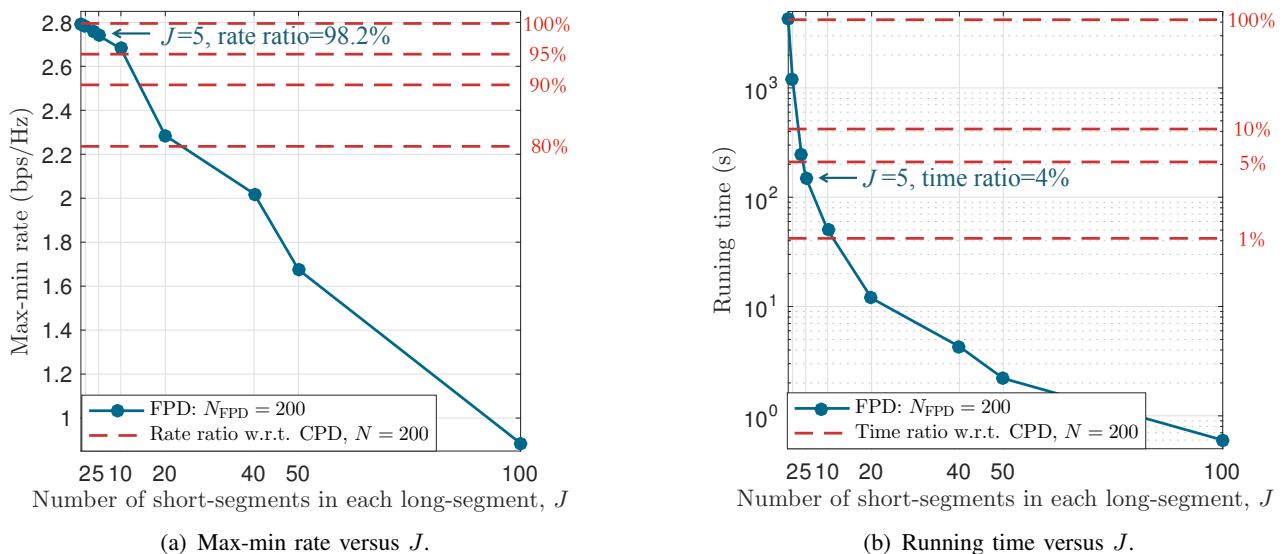


Fig. 6: Effects of parameter  $J$  on the performance of the proposed FPD scheme.

but slightly outperforms the latter when  $N > 200$  with even shorter algorithm running time. Moreover, compared to the CPD scheme, the proposed FPD scheme given the same number of (short-) segments (i.e.,  $N_{\text{FPD}} = N$ ) achieves very close max-min rate as the CPD scheme when  $N_{\text{FPD}} = N \geq 200$  (see Fig. 5(a)), while it takes much shorter running time of 1180 s versus 3954 s of the CPD (see Fig. 5(b)). However, the proposed FPD scheme suffers more severe rate performance loss than the CPD scheme when  $N_{\text{FPD}}$  is small. On the other hand, given the same number of designable waypoints for both the FPD and CPD schemes (i.e.,  $N_{\text{FPD}} = 2N$ ), the former scheme significantly outperforms the latter in terms of achievable rate (see Fig. 5(a)) while at the cost of comparable running time (see Fig. 5(b)). This is because given  $N_{\text{FPD}} = 2N$ , the UAV trajectory by the FPD scheme is composed of more waypoints (including both designable and non-designable ones) than the CPD scheme, which leads to longer path length in general and thus more DoF in the UAV trajectory design.

Figs. 6(a) and 6(b) show the effects of parameter  $J$  (i.e., number of short-segments in each long-segment) on the max-min rate and running time for the proposed FPD scheme given a fixed number of total short-segments  $N_{\text{FPD}} = 200$ . One can observe that as  $J$  increases, the max-min rate of the proposed FPD scheme monotonically decreases (see Fig. 6(a)), while its algorithm running time firstly drops quickly with  $J$  and then reduces slowly when  $J$  becomes large. This is expected since with larger  $J$ , fewer designable waypoints need to be optimized which leads to both rate performance degradation and running time reduction due to less DoF in the UAV trajectory design. Moreover, note that compared to the CPD scheme with the same number of total waypoints  $N + 1 = 201$ , the proposed FPD scheme with  $J = 5$  and hence only 41 designable waypoints attains more than 98% of the achievable rate of the



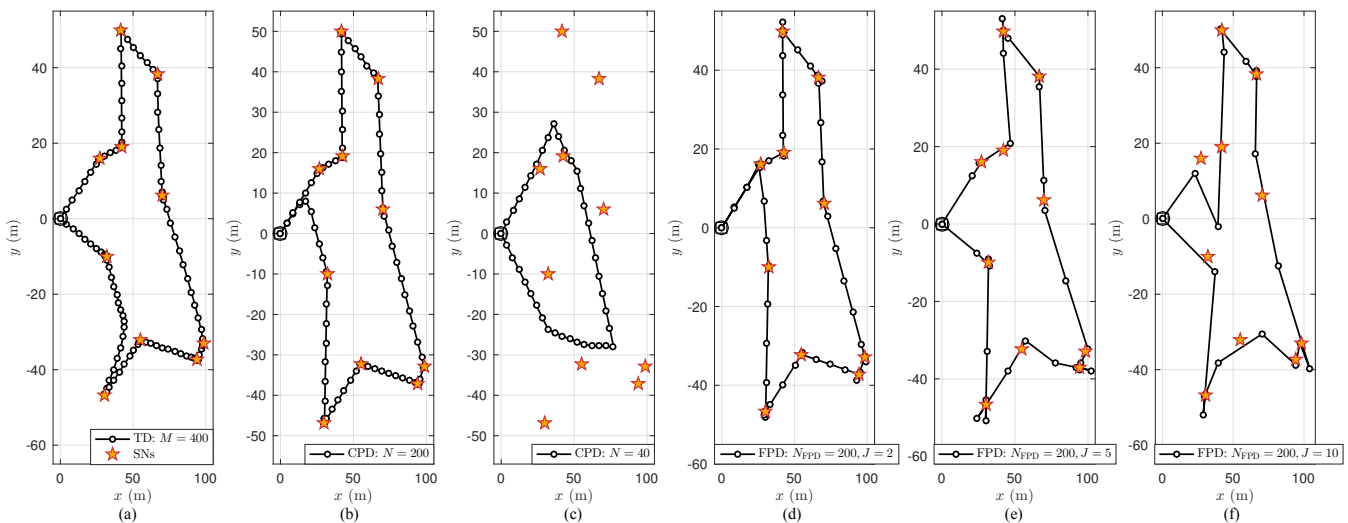


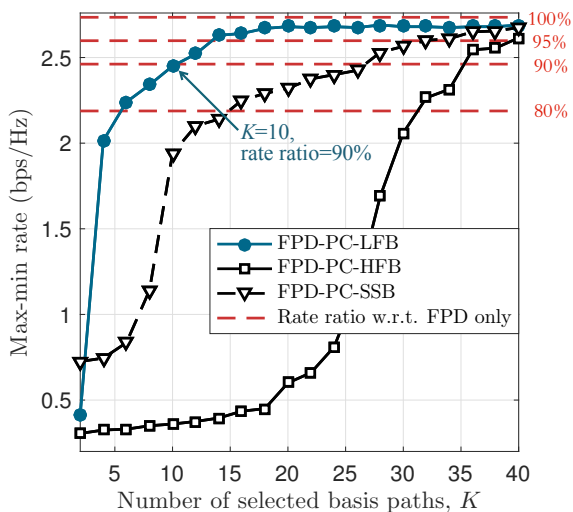
Fig. 7: Optimized UAV trajectories by different trajectory discretization schemes.

CPD scheme, while it takes only 4% of the running time of the CPD scheme. Such a result is appealing for practical implementation, which suggests that we can set small  $J$  for the FPD scheme to reap most of the rate performance by the CPD scheme but with substantially reduced running time.

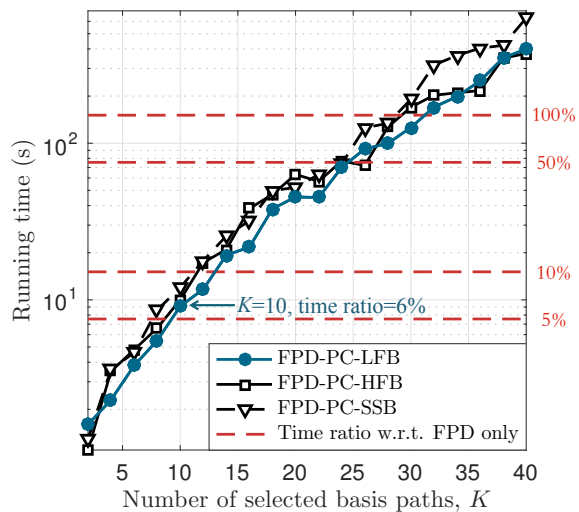
Fig. 7 plots the optimized UAV trajectories by different trajectory discretization schemes. First, it is observed that the optimized UAV trajectory by the CPD scheme with  $N = 200$  segments is similar to that of the TD scheme with much more segments,  $M = 400$ , both of which tend to sequentially travel nearby each SN (resembling the traveling-salesman-problem (TSP) solution [1]). Second, as  $J$  decreases, the optimized UAV trajectory by the proposed FPD scheme resembles that of the CPD scheme in the overall trajectory shape more closely. Specifically, with smaller  $J$ , the UAV trajectory is characterized by more designable waypoints, which allows the UAV to more flexibly control its trajectory nearby the SNs. Third, comparing Figs. 7(b) and 7(e), one can observe that given the same (small) number of designable waypoints (i.e.,  $N_{\text{FPD}}/J + 1 = N + 1 = 41$ ) and hence comparable algorithm running time, the optimized UAV trajectory by the proposed FPD scheme has more DoF to fly nearby the SNs for data collection than the CPD benchmark, since its trajectory consists of more (short-) segments and thus generally longer path length, which leads to larger max-min rate than the CPD scheme (cf. Fig. 5(a)).

### B. Performance of Proposed Path Compression

In Figs. 8(a) and 8(b), we compare the max-min rate and algorithm running time of the proposed FPD-PC scheme based on the first  $K$  (lowest-frequency) Fourier basis paths (named as FPD-PC-LFB) versus the number of selected basis paths ( $K$ ) against the following benchmark schemes: 1) FPD-PC-HFB: the FPD-PC scheme based on the last  $K$  (highest-frequency) Fourier basis paths; 2) FPD-PC-SSB:



(a) Max-min rate versus number of selected basis paths.



(b) Running time versus number of selected basis paths.

Fig. 8: Effects of parameter  $K$  on the performance of the proposed PC-FPD schemes.

the FPD-PC scheme based on the first  $K$  shifted-sine basis paths; 3) FPD only scheme (without PC). We consider  $N_{\text{FPD}} = 200$  and  $J = 5$  for all the schemes and have the following main observations. First, as  $K$  increases, the max-min rate for the FPD-PC-LFB and FPD-PC-SSB schemes firstly increases rapidly with  $K$  and then saturates when  $K$  becomes large; while their running time monotonically increases with  $K$ . The diminishing rate improvement can be explained by the similar reason given for Fig. 5(a). Second, the proposed FPD-PC-LFB scheme significantly outperforms the FPD-PC-HFB and FPD-PC-SSB schemes as it captures the main path features with low-frequency Fourier basis paths (see detailed reasons in the discussions for Fig. 4 in Section IV-B). Thirdly, with small  $K$  (e.g.,  $K = 10$ ), the proposed FPD-PC-LFB scheme attains nearly 90% of the max-min rate of the FPD only scheme (see Fig. 8(a)), while at the same time, it reduces about 94% of algorithm running time of the FPD only scheme (see Fig. 8(b)). This indicates that we can set small  $K$  for the proposed FPD-PC-LFB scheme in practice to substantially reduce the computational complexity of the FPD only scheme without scarifying rate performance notably. In addition, it is worth mentioning that given a relatively large  $K$  (e.g.,  $K \geq 30$ ), the proposed FPD-PC-LFB scheme incurs even long running time than the FPD only scheme, since the former scheme involves matrix operation and thus suffers higher computational complexity when  $K$  is too large.

Fig. 9 plots the optimized UAV trajectories by the FPD-PC scheme under different  $K$  and different basis paths as well as that by the FPD only scheme. All the UAV trajectories consist of  $N_{\text{FPD}} = 41$  designable waypoints. Comparing Figs. 9(a)–9(c), one can observe that the optimized trajectory by the proposed FPD-PC-LFB scheme approaches to that of the FPD only scheme (without PC) more closely

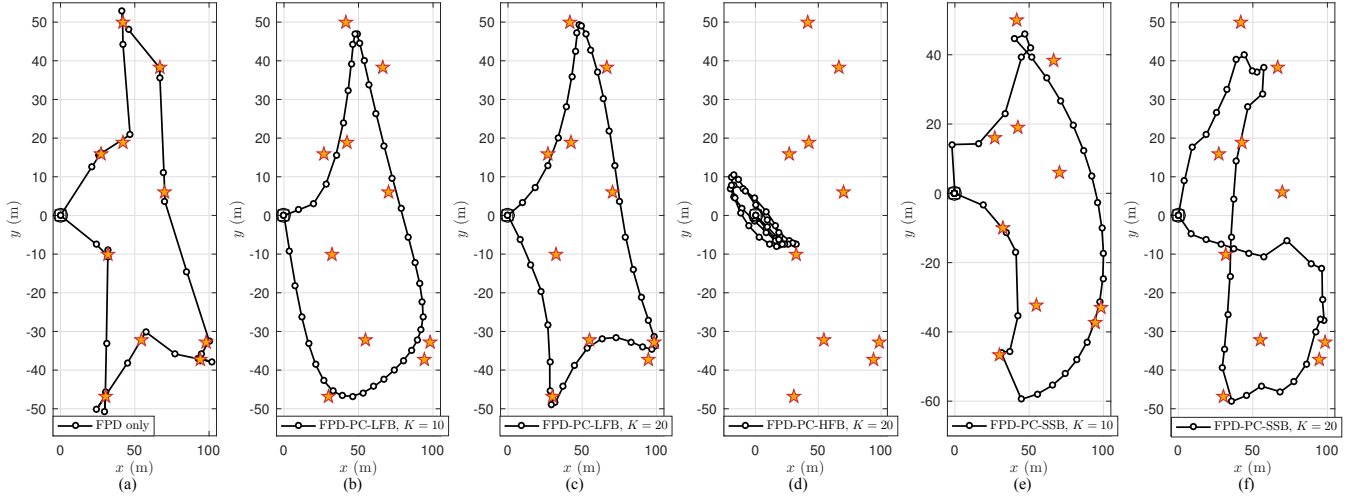


Fig. 9: Optimized UAV trajectories by different FPD-PC schemes.

when  $K$  is larger due to more basis paths selected. Next, it is observed in Fig. 9(d) that different from the FPD-PC-LFB scheme for which the UAV flies nearby the SNs for data collection, the UAV by the FPD-PC-HFB scheme, instead, sticks around the start location even given a relatively large  $K$  (e.g.,  $K = 20$ ). This is because high-frequency Fourier basis paths render the UAV trajectory with extremely fast path variation and thus can hardly constitute a smooth UAV path. Besides, given  $K = 10$  or  $K = 20$ , the optimized UAV trajectories by the FPD-PC-SSB scheme shown in Figs. 9(e) and 9(f), respectively, are far from optimal as compared to that in Fig. 9(a).

Last, we show in Fig. 10 the trade-off between rate performance and computational complexity for the proposed FPD-PC-LFB scheme by jointly adjusting the parameters  $J$  and  $K$ . The TD, CPD, and FPD only schemes are considered as benchmarks for comparison. It is observed that the combination of parameters  $\{J, K\}$  significantly affects the performance of the proposed FPD-FC-LFB scheme. On one hand, given the same  $K$ , it is necessary to properly set a modest value for  $J$  (e.g.,  $J = 4$ ) to achieve good rate performance although the schemes with different values of  $J$  incur comparable running time. This is because setting too small  $J$  (e.g.,  $J = 1$ ) results in a large number of designable waypoints in the UAV path, which cannot be well approximated by the fixed number of basis paths, thus leading to considerable rate performance loss; while setting too large  $J$  (e.g.,  $J = 10$ ) significantly limits the DoF in the UAV trajectory design (even without PC) since only a small number of designable waypoints are optimized. On the other hand, given a properly chosen  $J$  (e.g.,  $J = 4$ ), it is also necessary to set a proper  $K$  to balance the rate performance and design complexity trade-off. Similar observations can be made in Figs. 8(a) and 8(b) and thus are omitted for brevity.

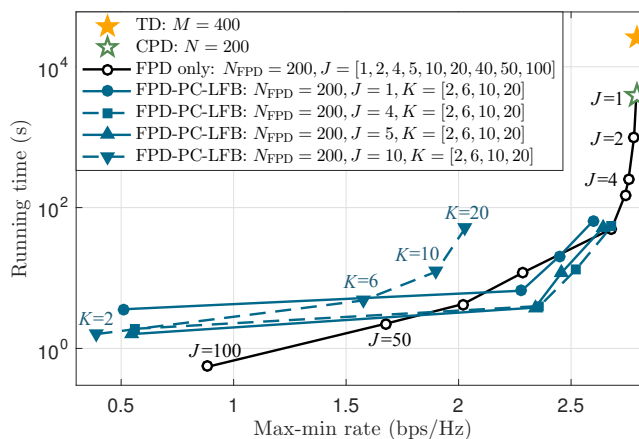


Fig. 10: The trade-off between rate performance and computational complexity for the proposed FPD-PC-LFB scheme.

## VII. CONCLUSIONS

In this paper, we proposed a new and general framework to reduce the computational complexity for the UAV trajectory and communication co-design over the existing TD and CPD schemes. Specifically, to reduce the number of waypoints to be optimized with CPD, we proposed an FPD scheme that optimizes only some of the waypoints (called *designable* waypoints) along the path for reducing the trajectory design complexity in the time domain, while all the waypoints (including both designable and non-designable ones) are used in calculating the approximated communication utility along the trajectory for ensuring high trajectory discretization accuracy. Moreover, given any number of designable waypoints, we proposed a novel PC scheme to further reduce the number of path design variables representing the designable waypoints by properly selecting a set of basis paths and approximating the path by a superposition of selected basis paths with optimized path coefficients. Numerical results showed that the proposed FPD and PC schemes significantly reduce the UAV trajectory design complexity yet achieve favorable rate performance as compared to TD and CPD schemes. The proposed framework is general and can be applied to design UAV trajectories under different channel models and for different purposes.

## APPENDIX

### A. Proof of Lemma 1

Let  $\Delta u_n$  denote the finite-sum approximation error for the utility function in segment  $n$ . Then we have

$$\begin{aligned} \Delta u_n &= \int_{t=0}^{t_n} u(\mathbf{q}_{n-1} + t\mathbf{v}_n) dt - t_n u(\mathbf{q}_n) = \int_{t=0}^{t_n} [u(\mathbf{q}_{n-1} + t\mathbf{v}_n) - u(\mathbf{q}_n)] dt \\ &\stackrel{(a_1)}{=} \int_{t=0}^{t_n} \nabla u(\mathbf{q}_{n-1} + \tilde{\mathbf{q}}_n)(t_n - t)\mathbf{v}_n dt \stackrel{(a_2)}{\leq} \int_{t=0}^{t_n} |\nabla u(\mathbf{q}_{n-1} + \tilde{\mathbf{q}}_n)\mathbf{v}_n|(t_n - t) dt \end{aligned}$$

$$\stackrel{(a_3)}{\leq} \int_{t=0}^{t_n} D_{u,n} \|\mathbf{v}_n\| (t_n - t) dt = \frac{1}{2} D_{u,n} \|\mathbf{v}_n\| t_n^2 = \frac{1}{2} D_{u,n} \Delta_n t_n, \quad (32)$$

where  $\tilde{\mathbf{q}}_n = t_0 \mathbf{v}_n$  with  $t_0 \in [0, t_n]$ ,  $\nabla u$  denotes the gradient of function  $u(\cdot)$  w.r.t.  $\mathbf{q}$ ,  $\Delta_n = \|\mathbf{v}_n\| t_n$  is the length of segment  $n$ ,  $D_{u,n} = \max_{\mathbf{q}=\mathbf{q}_{n-1}+t_0\mathbf{v}_n, t_0 \in [0, t_n]} \|\nabla u(\mathbf{q})\|$ . Note that  $(a_1)$  follows from the Rolle mean value theorem, the equality in  $(a_2)$  holds when  $\nabla u(\mathbf{q}_{n-1} + \tilde{\mathbf{q}}_n) \mathbf{v}_n \geq 0$ , and the equality in  $(a_3)$  holds when  $\nabla u(\mathbf{q}_{n-1} + \tilde{\mathbf{q}}_n)$  is constant over segment  $n$  and the vectors of  $\nabla u$  and  $\mathbf{v}_n$  align in the same direction. Thus, the finite-sum approximation error over the entire UAV trajectory  $\mathbf{q}(t)$  is

$$E_U = |U(\mathbf{q}(t)) - \bar{U}_{\text{CPD}}(\{\mathbf{q}_n\}, \{t_n\})| = \left| \sum_{n=1}^N \Delta u_n \right| \leq \sum_{n=1}^N \frac{1}{2} D_{u,n} \Delta_n t_n \leq \frac{1}{2} D_u \Delta_{\max}^U T, \quad (33)$$

where  $D_u = \max_n D_{u,n}$ , thus completing the proof.

### B. Proof for Example 1

Consider the achievable rate for the UAV at the location  $\mathbf{q} = [q_x, q_y, q_z]$ , given as

$$u(\mathbf{q}) = \log_2 \left( 1 + \frac{P\beta_0}{\|\mathbf{q} - \mathbf{w}\|^2 \sigma^2} \right) = \log_2 \left( 1 + \frac{P\beta_0}{[(q_x - w_x)^2 + (q_y - w_y)^2 + q_z^2] \sigma^2} \right). \quad (34)$$

With  $q_z \geq H_{\min}$ , it can be shown that  $\|\nabla u(\mathbf{q})\|$  takes its maximum value when  $q_z = H_{\min}$  and  $(q_x - w_x)^2 + (q_y - w_y)^2 = c_1^2$ , where  $c_1^2 = \frac{-(2H_{\min}^2 + c_2) + \sqrt{(16H_{\min}^4 + 16c_2H_{\min}^2 + c_2^2)}}{6}$  and  $c_2 = \frac{P\beta_0}{\sigma^2}$ . Thus, we have  $D_u = \max_{\tilde{\mathbf{q}} \in \mathbf{q}(t)} \|\nabla u(\tilde{\mathbf{q}})\| = \frac{2c_2}{\ln 2} \frac{c_1}{(c_1^2 + H_{\min}^2)(c_1^2 + H_{\min}^2 + c_2)}$ , thus completing the proof.

## REFERENCES

- [1] Y. Zeng, Q. Wu, and R. Zhang, "Accessing from the sky: A tutorial on UAV communications for 5G and beyond," *Proc. IEEE*, vol. 107, no. 12, pp. 2327–2375, Dec. 2019.
- [2] Y. Zeng, R. Zhang, and T. J. Lim, "Throughput maximization for UAV-enabled mobile relaying systems," *IEEE Trans. Commun.*, vol. 64, no. 12, pp. 4983–4996, Dec. 2016.
- [3] J. Chen and D. Gesbert, "Efficient local map search algorithms for the placement of flying relays," *IEEE Trans. Wireless Commun.*, vol. 19, no. 2, pp. 1305–1319, Feb. 2020.
- [4] Z. Kang, C. You, and R. Zhang, "3D placement for multi-UAV relaying: An iterative Gibbs-sampling and block coordinate descent optimization approach," *arXiv preprint arXiv:2006.09658*, 2020.
- [5] Y. Chen, W. Feng, and G. Zheng, "Optimum placement of UAV as relays," *IEEE Commun. Lett.*, vol. 22, no. 2, pp. 248–251, Feb. 2017.
- [6] C. Zhan, Y. Zeng, and R. Zhang, "Energy-efficient data collection in UAV enabled wireless sensor network," *IEEE Wireless Commun. Lett.*, vol. 7, no. 3, pp. 328–331, Jun. 2018.
- [7] Q. Wu, Y. Zeng, and R. Zhang, "Joint trajectory and communication design for multi-UAV enabled wireless networks," *IEEE Trans. Wireless Commun.*, vol. 17, no. 3, pp. 2109–2121, Mar. 2018.
- [8] Q. Wu, J. Xu, and R. Zhang, "Capacity characterization of UAV-enabled two-user broadcast channel," *IEEE J. Sel. Areas Commun.*, vol. 36, no. 9, pp. 1955–1971, Sep. 2018.

- [9] J. Gong, T.-H. Chang, C. Shen, and X. Chen, "Flight time minimization of UAV for data collection over wireless sensor networks," *IEEE J. Sel. Areas Commun.*, vol. 36, no. 9, pp. 1942–1954, Sep. 2018.
- [10] C. You and R. Zhang, "3D trajectory optimization in Rician fading for UAV-enabled data harvesting," *IEEE Trans. Wireless Commun.*, vol. 18, no. 6, pp. 3192–3207, Jun. 2019.
- [11] C. You and R. Zhang, "Hybrid offline-online design for UAV-enabled data harvesting in probabilistic LoS channel," *IEEE Trans. Wireless Commun.*, vol. 13, no. 6, pp. 3753–3768, Mar. 2020.
- [12] J. Xu, Y. Zeng, and R. Zhang, "UAV-enabled wireless power transfer: Trajectory design and energy optimization," *IEEE Trans. Wireless Commun.*, vol. 17, no. 8, pp. 5092–5106, Aug. 2018.
- [13] Y. Hu, X. Yuan, J. Xu, and A. Schmeink, "Optimal 1D trajectory design for UAV-enabled multiuser wireless power transfer," *IEEE Trans. Commun.*, vol. 67, no. 8, pp. 5674–5688, Aug. 2019.
- [14] Y. Zeng, J. Lyu, and R. Zhang, "Cellular-connected UAV: Potential, challenges, and promising technologies," *IEEE Wireless Commun.*, vol. 26, no. 1, pp. 120–127, Feb. 2018.
- [15] S. Zhang, Y. Zeng, and R. Zhang, "Cellular-enabled UAV communication: A connectivity-constrained trajectory optimization perspective," *IEEE Trans. Commun.*, vol. 67, no. 3, pp. 2580–2604, Mar. 2018.
- [16] W. Mei and R. Zhang, "Uplink cooperative NOMA for cellular-connected UAV," *IEEE J. Sel. Topics Signal Process.*, vol. 13, no. 3, pp. 644–656, Jun. 2019.
- [17] M. Hua, Y. Wang, Z. Zhang, C. Li, Y. Huang, and L. Yang, "Power-efficient communication in UAV-aided wireless sensor networks," *IEEE Commun. Lett.*, vol. 22, no. 6, pp. 1264–1267, June 2018.
- [18] F. Zhou, Y. Wu, R. Q. Hu, and Y. Qian, "Computation rate maximization in UAV-enabled wireless-powered mobile-edge computing systems," *IEEE J. Sel. Areas Commun.*, vol. 36, no. 9, pp. 1927–1941, Sep. 2018.
- [19] M. Mozaffari, W. Saad, M. Bennis, and M. Debbah, "Optimal transport theory for power-efficient deployment of unmanned aerial vehicles," in *Proc. IEEE Intl. Conf. Commun. (ICC)*, May 2016, pp. 1–6.
- [20] M. Mozaffari, W. Saad, M. Bennis, and M. Debbah, "Drone small cells in the clouds: Design, deployment and performance analysis," in *Proc. IEEE Global Commun. Conf. (Globecom)*, Dec. 2015, pp. 1–6.
- [21] J. Lyu, Y. Zeng, R. Zhang, and T. J. Lim, "Placement optimization of UAV-mounted mobile base stations," *IEEE Commun. Lett.*, vol. 21, no. 3, pp. 604–607, Mar. 2017.
- [22] M. Alzenad, A. El-Keyi, and H. Yanikomeroglu, "3-D placement of an unmanned aerial vehicle base station for maximum coverage of users with different QoS requirements," *IEEE Wireless Commun. Lett.*, vol. 7, no. 1, pp. 38–41, Feb. 2018.
- [23] J. Zhang, Y. Zeng, and R. Zhang, "Receding horizon optimization for energy-efficient UAV communication," *IEEE Wireless Commun. Lett.*, vol. 9, no. 4, pp. 490–494, Apr. 2019.
- [24] J.-H. Lee, K.-H. Park, Y.-C. Ko, and M.-S. Alouini, "A UAV-mounted free space optical communication: Trajectory optimization for flight time," *IEEE Trans. Wireless Commun.*, vol. 19, no. 3, pp. 1610–1621, Mar. 2020.
- [25] Y. Guo, S. Yin, J. Hao, and Y. Du, "A novel trajectory design approach for UAV based on finite Fourier series," *IEEE Wireless Commun. Lett.*, vol. 9, no. 5, pp. 671–674, May 2020.
- [26] C. Shen, T.-H. Chang, J. Gong, Y. Zeng, and R. Zhang, "Multi-UAV interference coordination via joint trajectory and power control," *IEEE Trans. Signal Process.*, vol. 68, pp. 843–858, Jan. 2020.
- [27] K. Xu, M.-M. Zhao, Y. Cai, and L. Hanzo, "Low-complexity joint power allocation and trajectory design for UAV-enabled secure communications with power splitting," *arXiv preprint arXiv:2008.10015*, 2020.
- [28] A. Ben-Tal and A. Nemirovski, *Lectures on modern convex optimization: Analysis, algorithms, and engineering applications*. Siam, 2001, vol. 2.
- [29] M. Grant, S. Boyd, and Y. Ye, "CVX: Matlab software for disciplined convex programming," 2008.